https://doi.org/10.5194/egusphere-2026-2314
Preprint. Discussion started: 22 June 2026

Arctic coastal reactors: Lateral and vertical organic matter dynamics in permafrost lagoons of the western Canadian Arctic

George Tanski[1,2,3], Michael Fritz[1], Jorien E. Vonk[2], Jens Strauss[1], Léo Chassiot[4], Vladislav Carnero-Bravo[5,6], Jade Falardeau[5], Konstantin Klein[1,7], Patrick Lajeunesse[4], Hugues Lantuit[1,7], Niek J. Speetjens[2], Anne de Vernal[5], Dustin Whalen[3], and Anna M. Irrgang[1]*

[1] Permafrost Research Section, Alfred Wegener Institute Helmholtz Centre for Polar and Marine Research, Potsdam, Germany
[2] Department of Earth Sciences, Vrije Universiteit Amsterdam, Amsterdam, The Netherlands
[3] Natural Resources Canada, Geological Survey of Canada–Atlantic, Dartmouth, Canada
[4] Department of Geography, Université Laval, Québec City, Canada
[5] Geotop Research Center in Earth System Dynamics, Département des Sciences de la Terre et de l'Atmosphère, Université du Québec à Montréal, Montréal, Canada
[6] Instituto de Ecología, Universidad del Mar, Campus Puerto Ángel, Puerto Ángel, Oaxaca, México
[7] Institute for Geosciences, Universität Potsdam, Potsdam, Germany

Correspondence to: Anna M. Irrgang (anna.irrgang@awi.de)

Abstract. Arctic warming leads to longer open-water periods, intensified storms, and rising relative sea level, which accelerate permafrost coastline erosion and enhance the lateral transport of sediment and organic matter (OM) from land to sea. Lagoons and embayments are widespread along Arctic coasts, and are located at the heart of the land-sea transition zone, yet their role in OM cycling remains poorly understood. Here, we assess the function of the Kanivaliuraq lagoon (Ptarmigan Bay, western Canadian Arctic) as a biogeochemical reactor for terrestrial OM. We combine shoreline position changes (1950–2018) with sediment core and surface sediment transect sampling to quantify sources, pathways, and trajectories of OM and sediments. Samples were analyzed for total organic carbon (TOC), total nitrogen, stable carbon isotopes ($\delta^{13}C$), mineral surface area, and grain size, complemented by sedimentation rates from 210Pb/137Cs dating and water turbidity dynamics from Landsat imagery. We find that OM content declines by more than 50% along the land–lagoon–ocean gradient, both in TOC (% dry weight) and OC loading (mg OC m^{-2}), indicating efficient degradation, burial and offshore transport of terrestrial OM within the lagoon. While currents and wind-driven resuspension are expected to further enhance OM redistribution and export, a substantial amount of OM is sequestered and mineralized in lagoon sediments reflecting both effective burial and degradation of erosion-derived OM. Yet, a major portion of OM is also quickly removed offshore. Shoreline erosion rates increased from 0.6 m yr^{-1} in the 1950s to 0.9 m yr^{-1} in the 1970s to 3.3 m yr^{-1} in 2011 to 2018, paralleled by increasing mass accumulation rates from 0.32 to 0.57 g cm^{-2} yr^{-1}. Due to intensified erosion and warming-induced permafrost degradation, lagoons and embayments will be supplied with increasing amounts of terrestrial OM being subject to either mineralization, sequestration or offshore transport, also fueling primary production in these Arctic coastal "reactors" at the same time. Our results highlight that Arctic lagoons, often overlooked components of the land–ocean transition zone, act as dynamic reactors and partial sinks for terrestrial OM. Intensifying coastal erosion as a result of Arctic climate warming is likely to increase their importance in Arctic carbon cycling.

https://doi.org/10.5194/egusphere-2026-2314
Preprint. Discussion started: 22 June 2026

1. Introduction

Since the late 1970s, the Arctic has been warming nearly four times more than the global mean (Rantanen et al., 2022). This warming has significant and wide-ranging impacts on both terrestrial and marine ecosystems. It impacts previously frozen carbon stocks on land (Schuur et al. 2022, Strauss et al. 2025) and beneath the seafloor (Miesner et al., 2023), and alters biogeochemical pathways (Natali et al., 2019; Turetsky et al., 2020; AMAP, 2021; Rößger et al., 2022).

One of the most pronounced consequences is the accelerated warming of permafrost, resulting in widespread thaw across the circumpolar region (Biskaborn et al., 2019; Schuur et al, 2022). In parallel, Arctic coastal zones are undergoing rapid environmental transformation, driven by longer open water seasons, intensified storms and relative sea level rise (Creel et al., 2024; Overeem et al., 2011; Casas-Prat and Wang, 2020; Falardeau et al., 2023a). These trends have the potential to accelerate the erosion of permafrost coasts and are projected to intensify in the future (Barnhart et al., 2014; Farquharson et al., 2018; Irrgang et al., 2018, 2022; Jones et al., 2018; Nielsen et al., 2022), leading to increased lateral fluxes of sediment, carbon, and nutrients from land to sea (Vonk et al., 2012; Wegner et al., 2015; Fritz et al., 2017; Couture et al., 2018; Vonk et al., 2025).

Arctic lagoons play a particularly important role in the carbon and nutrient cycles of the land-ocean continuum. They function as zones of production, degradation, retention and transport of OM along lateral and vertical pathways (Dunton et al., 2006; Schirrmeister et al., 2018; Jenrich et al., 2021). They form a part of the inner shelf and are important interceptors for terrestrially-derived OM and sediments (Solomon et al., 2000; Schreiner et al., 2013; Hanna et al., 2014; Harris et al., 2018). While offshore shelf areas typically serve predominantly as sinks for terrestrial OM, biogeochemical processes within lagoons are more complex and dynamic (Hanna et al., 2014; Evans et al., 2021).

Recent research has increasingly focussed on permafrost lagoons, particularly thermokarst lagoons (Schirrmeister et. al, 2018; Jenrich et al. 2025a, b, c). Jenrich et al. (2025c) mapped and classified 520 thermokarst lagoons along the coastline of five Arctic shelf seas (Laptev, East Siberian, Chukchi, Alaskan Beaufort and Canadian Beaufort seas) between the Taymyr and Tuktoyaktuk peninsulas, and most were located along the Canadian Beaufort Sea. Coastal erosion and sea level rise can breach lakes, drained lake basins or low-lying coastal permafrost terrain, converting them into coastal lagoons and embayments. This process is highly dynamic because coastal features change drastically on centennial and millennial scales (Creel et al., 2024). In addition, rivers (even small or ephemeral) and streams can provide sediment and gravel supporting the development of spits, which can host and trap eroded material and OM. These lagoons, regardless of their origin, act as dynamic transition zones between terrestrial and marine environments (Jenrich et al., 2025). Seawater intrusion into frozen sediments accelerates permafrost thaw, exposing formerly frozen or buried OC. This carbon then becomes available for microbial decomposition, resulting in the release of greenhouse gases (GHGs) which fuels the permafrost carbon feedback, ultimately contributing to further warming (Schuur et al., 2015).

Although lagoons are widespread features of the Arctic land–ocean transition zone, their role in biogeochemical cycles and carbon budgets remains poorly constrained, with only a limited number of studies addressing their role in the carbon cycle (Jenrich et al., 2021). Along the northwestern Canadian and US American Arctic coast, shallow estuarine lagoons are a prevalent feature of the land-ocean transition zone. Harris et al. (2017) estimate that lagoons constitute more than 70% of the eastern Alaskan Beaufort Sea coastline. More recent mapping and classification by Jenrich et al. (2025) highlights their extensive distribution throughout the western Canadian Arctic, with an average density of ~0.86 lagoons per kilometer along the Yukon coast. Both open and closed lagoons are present along the Yukon coast, forming the transition zone to the narrow shelf of the Beaufort Sea (Fig. A1). Between

https://doi.org/10.5194/egusphere-2026-2314
Preprint. Discussion started: 22 June 2026

the Alaskan border and the Babbage River, lagoons occupy approximately 60 km of the coastline, corresponding to about 20% of the total Yukon coastline (Forbes, 1997; Couture et al., 2018). These numbers represent a first-order estimate derived from geomorphological coastline segmentation rather than a dedicated lagoon inventory.

Shallow lagoon deposits are particularly susceptible to reactivation under changing environmental conditions in the Arctic. Prolonged open-water periods promote winnowing, resuspension, and transport, increasing the mobility of OM and sediments. Within this dynamic context, lagoons act as natural biogeochemical reactors, processing both terrestrial and marine-derived OM and potentially enhancing the production of climate-relevant greenhouse gases (GHGs) (Schirrmeister et al., 2018). Methane (CH_4) production observed in Siberian thermokarst lagoons (Jenrich et al., 2025a) and potential carbon dioxide (CO_2) production in nearshore sediments in the Canadian Arctic indicate intensive degradation of OC resulting in potential venting of GHG into the atmosphere (Tanski et al., 2019).

Despite their abundance and significance within the land–ocean continuum, Arctic lagoons have received considerably less attention than rivers or the open shelf in carbon cycling studies. In this study, we examine the role of Arctic lagoons as reactors of terrestrial OM in the Arctic land-to-ocean continuum. We seek to assess sources, quantities, and transport pathways of OM during its transition from the terrestrial to the marine environment. Specifically, we aim to (i) quantify long-term sediment and OM fluxes resulting from shoreline erosion, (ii) quantify sediment and OM accumulation rates in lagoons, and (iii) assess the lateral and vertical dynamics of OM within lagoons, which relate to transport, burial, and degradation. By addressing these objectives, we seek to advance the understanding of Arctic lagoons as active reactors of OM and their role in the Arctic carbon cycle.

Study Area

The study area is located along the Yukon coast in the western Canadian Arctic, which stretches approximately 300 km from the Mackenzie Delta to the Alaskan border (Fig. 1). The Yukon Coastal Plain is characterized by continuous permafrost with a shallow seasonal active layer of ~30-50 cm (Wagner et al., 2026; Wolter et al., 2018) and is composed of various Quaternary deposits of lacustrine, fluvial, colluvial and glacial origin (Rampton, 1982; Fritz et al., 2012). During the Wisconsin glaciation (~75,000 to 11,000 years ago) of the late Pleistocene, the lagoon area was covered by the Laurentide Ice Sheet extending from the east as far as the Firth River (Fig. 1) (Mackay, 1959; Rampton, 1982). Permafrost in previously glaciated terrain is ice-rich throughout the Yukon Coastal Plain. Ground ice occupies on average 46% of the upper permafrost volume, ranging from ~3% in gravel deposits of barrier islands and spits to ~54% in fine-grained lacustrine deposits (Couture et al., 2018). Massive ground ice structures are widely distributed over the Yukon Coastal Plain together with ice wedges, segregated ice and buried glacier ice in the formerly glaciated part of the Yukon coast (Fritz et al., 2012; Couture and Pollard, 2017). The polygonal tundra is intersected by small streams and rivers. The open water season lasts for approximately four months and sets in earlier towards the Mackenzie Delta, where relatively warm water masses reach the coast during the spring freshet and later towards Herschel Basin, where land-fast ice is more persistent (Carmack and Macdonald, 2002; Dunton et al., 2006; Falardeau, 2023a). The Mackenzie River plume strongly influences the coastal waters in the wider study area by providing large amounts of fresh water, fine sediments and terrestrial OM (Macdonald et al., 1998, 2015; Tank et al., 2016; Juhls et al., 2022). The wind direction is bi-modal and coming mostly from east-southeast (ESE), or northwest (NW) and influences water temperature, turbidity and OM dispersal from the Mackenzie River towards the study area (Hill et al., 1991; Matsuoka et al., 2012; Klein et al., 2019). Astronomical tides in the region are semidiurnal and in the microtidal range (20 to 80 cm) (Canadian Hydrographic Service, 2022). During storm surges

https://doi.org/10.5194/egusphere-2026-2314
Preprint. Discussion started: 22 June 2026

water levels can rise more than 1 m above mean sea level (Forbes, 1997; Manson and Solomon, 2007). Coastal erosion rates are on average 0.7 m yr^{-1} with extreme rates of > 20 m yr^{-1} at certain locations (Irrgang et al., 2018; Obu et al., 2017).

Along the Yukon coast various types of lagoons and bays exist (Couture et al., 2018; Irrgang et al., 2018). They range from semi-open barrier systems that developed in front of river deltas such as the Firth and Malcolm River (Nunaluk spit) and the Babbage River (Philipps Bay) to semi-open or closed lagoons such as Whale Bay, Roland Bay or King Point (Figs. 1, A1).

Our area of investigation is Kanivaliuraq lagoon, also known as Ptarmigan Bay. Kanivaliuraq lagoon is located in close proximity to Qikiqtaruk (also known as Herschel Island) (Fig. 1, A1). The lagoon is enclosed by an approximately 5 km long gravel spit, which grows constantly towards the northwest since the 1950s (Forbes, 1997; Irrgang et al., 2018). The lagoon is mostly shallow (<1 m water depth) and has a ~3 m deep channel (see Fig. A2), which is situated close to the gravel spit. The inner part of the lagoon is characterized by intensive coastal erosion (Forbes, 1997; Irrgang et al., 2018). A small creek, referred to as Black Creek (Speetjens et al., 2022), draining a catchment of 4 km², is located at the enclosed southern end of the lagoon (Fig. 1). Numerous driftwood logs are present in the enclosed part of the lagoon. The proximate hinterland of the lagoon is characterized by a low topography with wetlands but rises continuously towards the foothills of the Richardson Mountains (Forbes, 1997). Towards the northwest, the lagoon opens to the Workboat Passage and Herschel Basin (Fig. 1). The nearshore currents in Workboat Passage transport water masses dominantly from west to east with further water masses transported from north to south along the eastern coast of Qikiqtaruk towards Kanivaliuraq lagoon at the mainland (Dunton et al., 2006; Radosavljevic et al., 2022).

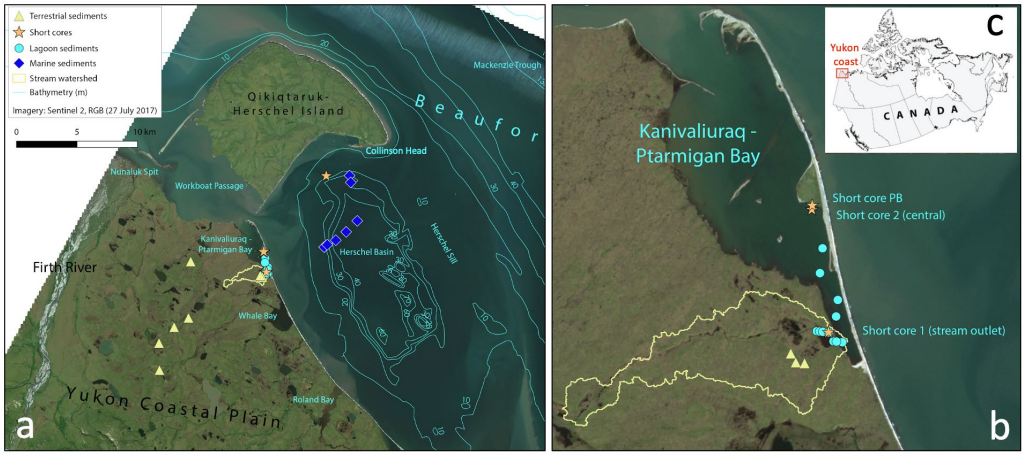

Fig. 1. (a) Study area map with sampling sites on the Yukon coast including Kanivaliuraq – Ptarmigan Bay lagoon and Herschel Basin in the western Canadian Arctic. Sediment samples were taken from terrestrial, lagoon and marine sites. Bathymetry gives the water depth below sea surface in metres. (b) Close-up of the Kanivaliuraq – Ptarmigan Bay lagoon with Black Creek watershed outlined in yellow, and (c) study area location. Map modified from Speetjens et al. (2022). Background imagery: Sentinel-2 satellite imagery, RGB composite (Copernicus Programme, European Space Agency), acquired on 27 July 2017.

https://doi.org/10.5194/egusphere-2026-2314
Preprint. Discussion started: 22 June 2026

2. Methods

2.1 Shoreline change analyses

Shoreline change rates were obtained following the methodology described in Irrgang et al. (2018). Aerial imagery from the years 1953 and 1972 was co-georeferenced to the geo-located GeoEye-1 satellite images with a spatial resolution of 0.5 m from 2011. In addition to the data provided in Irrgang et al. (2018), Pléiades imagery from 2018 with a resolution of 2 m was used to extend the shoreline change calculations to 2018. Shorelines were digitized manually from the aerial imagery and satellite imagery at a scale of 1:1000 by an experienced operator, using the vegetation line as a shoreline proxy. For the calculation of shoreline change rates, the Esri ArcGIS software extension tool DSAS (Digital Shoreline Analysis System) version 5.0 was used (Himmelstoss et al., 2018). DSAS uses a manually delineated baseline (in this study the inland of the shorelines) as a starting point to draw perpendicular transects at a designated spacing, here set to 50 m. The distance of the shorelines to each other is calculated from the position of the intersection points in between transects and the shorelines. For this study, we used the end point rate method, which gives the average distance in metres per year. We performed this calculation for each time step separately, resulting in four time steps: 1953-1972, 1972-2011, 2011-2018, and 1953-2018. For Qikiqtaruk, no imagery from the 1950s was available, resulting in three time steps.

2.2 Surface water turbidity

Turbidity and water temperature were modelled based on the methodology presented in Klein et al. (2019). Cloud- and ice-free level 1T Landsat (TM, ETM+, OLI/TIRS, 20 m resolution) acquisitions were selected, then sorted based on the wind conditions at the acquisition day, and downloaded from the United States Geological Service (USGS, 2022). The dataset contains data from 1990 to 2016. Wind data were downloaded from the Qikiqtaruk and Komakuk Beach weather stations from the climate archive of Environment Canada Canada (Government of Canada, 2022). In total, we used 26 Landsat images for the analyses. Of these, 18 images that showed stable ESE wind conditions and 8 showed stable NW wind conditions. Landsat level 1T data did not receive any processing except for georeferencing prior to download. Atmospheric Correction was performed using the ACOLITE Software (Vanhellemont 2019) prior to modelling turbidity according to Klein et al. (2021) by applying the Arctic Nearshore Turbidity Algorithm (ANTA). Water temperature was calculated from thermal infrared channels using radiance add, radiance multiplier and two sensor specific thermal constants, which are all given in the Landsat metadata (Wukelic et al., 1989). The resulting brightness temperatures are not surface temperatures, but show adequate accuracy (~1K) for relative comparison and are thus sufficient for this study. The resulting turbidity (FNU) and water temperature (°C) images were aggregated according to their wind regime and mean values for each pixel were calculated to map the representative ESE and NW wind conditions.

2.3 Sediment sampling

Sampling took place in 2016, 2018, and 2019 and targeted terrestrial, lagoon and marine sediments on the Yukon Coastal Plain, Kanivaliuraq (Ptarmigan Bay) lagoon and Herschel Basin (Fig. 1 and Fig. A1), respectively. Terrestrial sediments included the seasonally unfrozen layer (i.e., active layer) and upper permafrost, which we sampled in August 2018. Lagoon surface sediments, lagoon short cores and the marine short core in Herschel Basin were taken in the same season. Additional material from marine short cores was used (Grotheer et al., 2020; Fig. 1). The terrestrial sediments close to the shore of the lagoon (n= 14) were sampled

https://doi.org/10.5194/egusphere-2026-2314
Preprint. Discussion started: 22 June 2026

near the outlet of the stream in a high-centered polygon field with a stainless steel cylinder and a Hilti drill. The other terrestrial samples (n= 10) include active layer and permafrost sediments taken with a SIPRE corer in spring 2019. Lagoon short cores were collected using a UWITEC percussion corer at two locations in the enclosed part of the lagoon and were sub-sampled at 1-cm intervals on site and then frozen. The first short core was taken close to the stream outlet (short core 1 - Stream Outlet, ~29 cm length), while the second short core was cored at ~2 km distance from the outlet in the central part of the lagoon (short core 2 - Central, ~23 cm length; see Fig. 1 and Table A1). At the same location of short core 2, the third core (short core YC18-PB-SC01; hereafter PB; see Fig. A1 and Table A1) was also taken with a percussion corer at 3 m water depth and a total length of ~64 cm of sediment was recovered. Lagoon surface sediments from the lagoon floor (n = 11) were taken with a Van Veen grab sampler along a surface sediment transect between the short core locations 1 and 2 following the channel from the stream outlet to the lagoon centre. The 38 cm-long marine short core YC18-HB-GC01 from Herschel Basin (hereafter HB) was retrieved with an UWITEC gravity corer at 18 m water depth (Table A1). The data on ^{210}Pb and ^{137}Cs for short core HB were taken from a shared dataset (Carnero-Bravo et al., 2021; Falardeau et al., 2023b). Marine sediments sampled in 2016 consisted of six short cores (blue diamonds in Figure 1; ~15-26 cm length, n= 152). Sediment subsamples were kept frozen until further analysis in the laboratories.

2.4 Chronology and mass accumulation rates

The chronology of PB and HB cores were determined from ^{210}Pb and ^{137}Cs records. For ^{210}Pb measurements, a spike of ^{209}Po (~0.1 g) was added to each sediment sample (~0.3 g) as internal control of radiochemistry-experiment recuperation for α-spectrometry (ORTEC™ silicon surface barrier detectors). Supported ^{210}Pb was obtained through the measurement of ^{226}Ra with γ-ray spectrometry (Canberra™ HPGe well detector) using the average activity of ^{214}Pb and ^{214}Bi. For gamma spectrometry, the samples were measured after they were dried and stored in sealed plastic containers at room temperature for at least 21 days. The age of sediment layers was calculated with a Constant Rate of Supply model (CRS; Sanchez-Cabeza and Ruiz-Fernandez, 2012). A constant flux - constant sedimentation model (CFCS; Abril-Hernández, 2023) was run on the PB core. The uncertainties for dates and mass accumulation rates were calculated with Monte Carlo simulation (Sanchez-Cabeza et al., 2014). ^{137}Cs was directly measured by γ-ray spectrometry and used as an independent chronology corroboration. We used two reference ages, i.e., the onset of ^{137}Cs activity after 1950 CE and the activity peak in 1963 CE (Kuzyk et al., 2013). Organic carbon mass accumulation rates (OC_{MAR}) are based on mass accumulation rates (MAR; taking dry bulk density and age into account) and TOC concentrations of each sediment layer, where available. A third-order polynomial fitting was used to fill data gaps in the sediment core analyses, either in TOC or in MAR.

2.5 Sedimentology

Grain size distribution (GSD) of lagoon surface sediments and lagoon short cores 1 (stream outlet) and 2 (central) were measured at the Alfred Wegener Institute (AWI) in Potsdam. Lagoon short core PB and marine short core HB were analysed at Université du Québec à Montréal (UQAM). For GSD at AWI in Potsdam, organic material was removed by treating approximately 5-10 g of freeze-dried sample with 30% H_2O_2 under constant movement on a shaking table for several weeks until the reaction with H_2O_2 ceased. Organic-free freeze-dried samples were homogenised, dispersed in 1 L of 0.01M NH_4OH and shaken for 24 hours to disperse sediment conglomerates. Afterwards, three replicates were measured with a laser diffraction particle analyser (Malvern Mastersizer 3000). At UQAM, around 1 g of dry sample was treated with 30% H_2O_2. Then, up to 80 mL water was added to the

https://doi.org/10.5194/egusphere-2026-2314
Preprint. Discussion started: 22 June 2026

samples and a subsample taken while the sample was being mixed on a vortex mixer and poured into the laser diffraction analyzer. Particle size distributions between 0.0128 and 1000 µm were processed with GRADISTAT Version 9.1 (Blott & Pye, 2001).

Mineral surface area (SA) was measured on the lagoon surface sediments. Sediments were freeze-dried and gently homogenised. Approximately 1-3 g of subsample were then combusted for 12 hours at 450°C to remove organic matter. Combusted sediments were rinsed two times with ultrapure water to remove salts and then freeze-dried. Before SA measurement, samples were degassed for ~2 hours at 300°C with a Nova 4200e surface area analyzer (Quantachrome). Mineral SA is given in $m^2\ g^{-1}$ and was analysed by sorption of liquid nitrogen after the 6-point Brunauer-Emmett-Teller method (Brunauer et al., 1938).

The quantitative X-ray diffraction (XRD) of bulk sediment (well ground and mixed) was used to obtain the main mineralogy composition (quartz, chlorite, illite, albite, calcite and dolomite). Analyses were done with a Siemens D500 X-Ray diffractometer, and the spectra were resolved with EVA Bruker-AXS software.

2.6 Bulk geochemistry

Bulk geochemical parameters include TOC, total nitrogen (TN) as well as stable carbon isotopes ($\delta^{13}C$) to characterise the OM. All terrestrial sediments, lagoon short core PB and marine short core HB were analysed at the Stable Isotope Facility (SIF) of the University of California, Davis (USA). Lagoon surface samples, lagoon short core 1 (stream outlet), short core 2 (central) and remaining marine short cores were measured at AWI Potsdam.

For analysis of TOC, TN, $\delta^{13}C$ at SIF, UC Davis, sediments were freeze-dried, homogenised and subsampled (~5-30 mg). All subsampled sediments were fumigated over hydrochloric acid (37%) for 72 hours at 60°C to remove inorganic carbon and dried over NaOH pellets for 1-2 days at the same temperature setting to remove all moisture. TOC and TN were analysed with an ECS 4010 Elemental Analyzer (Costech). Stable carbon isotopes were analysed with an Elementar Vario El Cube elemental analyser coupled to an Isoprime VisION IRMS (Elementar) or a PDZ Europa 20-20 isotope ratio mass spectrometer (Sercon).

At AWI Potsdam, TN contents were quantified on freeze-dried and homogenised sediments using a Vario EL III elemental analyzer (Elementar, Germany). TOC was analysed with a Vario Max C analyser (Elementar, Germany). Prior to TOC analysis, inorganic carbon was removed manually by acid treatment on the same subset of samples used for $\delta^{13}C$ analysis. For $\delta^{13}C$ analysis, carbonates were removed from the sediments with hydrochloric acid (1.3 molar) for three hours at 95°C. Isotope ratios were measured with a Delta-V-Advantage mass spectrometer (Thermo Fisher Scientific) connected to a CONFLO IV gas mixer. Stable $\delta^{13}C$ isotopes are reported in per mil (‰) with carbon isotopes given as $\delta^{13}C$ relative to the standard Vienna Pee Dee Belemnite (VPDB).

2.7 Estimation of OC pools, annual OC fluxes and OC burial

We estimated OC and nitrogen pools for the upper 30 cm in the terrestrial catchment and in lagoon sediments of the Kanivaliuraq lagoon – Ptarmigan Bay (PB), as well as in marine Herschel Basin (HB) sediments (Table 2). Terrestrial pools are from Wagner et al. (2023). PB (lagoon) and HB (marine) data are based on averages and standard deviations from the upper 30 cm in lagoon and marine sediment cores, respectively. We have chosen a consistent depth interval (0-30 cm), which is limited by marine sediment core depth, for better comparability of the data.

We calculated the mean annual soil organic carbon (SOC) fluxes by coastal erosion for each time period (1953-1972, 1972-2011, 2011-2018). We digitized the lagoon area from aerial imagery in 1953 and 1972 and from GeoEye imagery in 2011 and Pleiades imagery in 2018. We then matched the digitized polygons with the terrain units from Couture et al. (2018) and assigned the

https://doi.org/10.5194/egusphere-2026-2314
Preprint. Discussion started: 22 June 2026

attributes from those units in terms of coastal height and SOC values. The area loss was calculated for each terrain unit, for each time period and then multiplied with the unit-specific coastal height and SOC value. We then divided each time period by its respective number of years to assess mean annual SOC fluxes.

Mean mass accumulation rates (MAR) and OC mass accumulation rates (OC_{MAR}) for the Kanivaliuraq lagoon – Ptarmigan Bay (PB) and marine reference site Herschel Basin (HB) were calculated for the different periods between 1953 and 2018 CE that match periods with shoreline change rates. OC_{MAR} is based on mass accumulation rates (MAR; taking dry bulk density and age into account) and TOC concentrations of each sediment layer of the same depth interval, where available. A third-order polynomial fitting was used to fill data gaps in the sediment core analyses, either in TOC or in MAR. Mean MAR and OC_{MAR} (Table 1) are provided with ± standard deviation.

3. Results

3.1 Shoreline change rates

The mean shoreline change rates in Kanivaliuraq lagoon increased since the 1950s from -0.6 ± 0.8 m yr^{-1} (negative values indicating erosion) in the period from 1953-1972 to -0.9 ± 0.8 m yr^{-1} (1972-2011) and ultimately to -3.3 ± 0.7 m yr^{-1} in the latest observation period (2011-2018) with extreme rates of -21.7 m yr^{-1} in the last decade (Table A2 and Fig. 2a). At 29.8% of the shoreline transects observed, erosion was recorded in the 1953-1972 period, which rose to 70.6% in the period 2011-2018. Several parts of the shore within the lagoon were affected by intensive shoreline retreat. In contrast, the gravel spit which is bordering the lagoon towards the east, expanded in north-western direction, which resulted in a narrowing of the lagoon inlet corridor over time.

At Qargialuk (also known as Catton Point), which is situated in close proximity to short core PB (Fig. 2b), mean shoreline change rates increased since the 1972-2011 period from -0.2 ± 0.3 m yr^{-1} to -0.5 ± 0.7 m yr^{-1} during the period 2011-2018. However, shoreline change rates were highest during the 1953-1972 period reaching on average -0.9 ± 0.8 m yr^{-1}. At Qargialuk no significant shoreline erosion took place in the time period 2011-2018 and approximately 50% (1953-1972) and 25% (1972-2011) of the shoreline was erosive during earlier decades.

Shoreline change rates along the south-eastern part of Qikiqtaruk (Fig. 2c, d) remained mostly stable since the 1970s. In the 1972-2011 period, rates were -0.6 ± 0.3 m yr^{-1} and increased only slightly to -0.7 ± 0.7 m yr^{-1} during the period 2011-2018. Although shorelines recording significant erosion decreased from the 1972-2011 (~68%) to the 2011-2018 period (~47%), highest erosion rates were recorded during 2011-2018 with rates up to -5.8 m yr^{-1}. The eastern part of the coast, characterized by an alluvial fan and high bluffs (known as Collinson Head), was especially affected by strong erosion (Figs. 1, 2c, d).

https://doi.org/10.5194/egusphere-2026-2314
Preprint. Discussion started: 22 June 2026

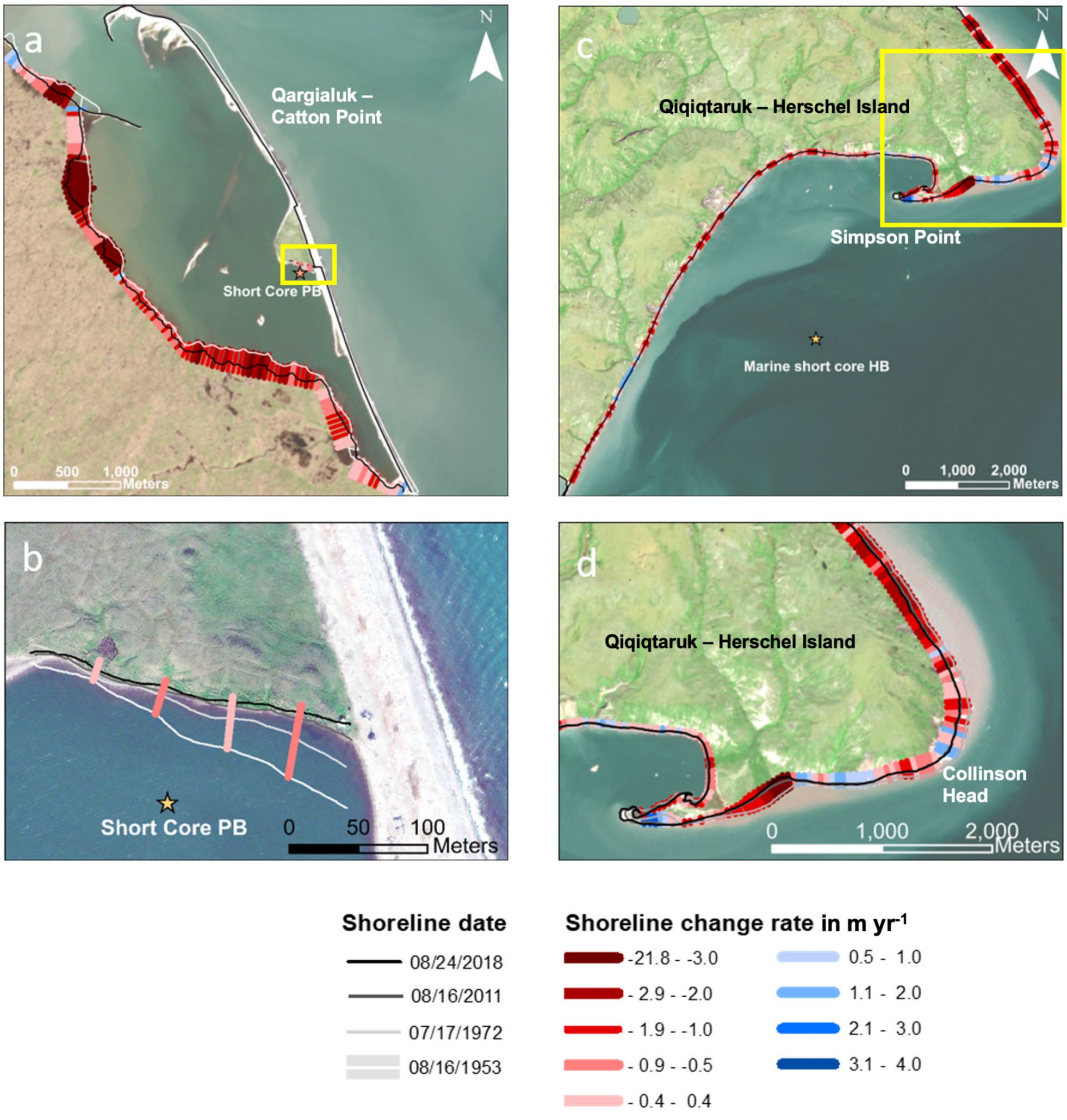

Fig. 2. Shoreline positions and mean shoreline change rates between 1953 and 2018 for Kanivaliuraq – Ptarmigan Bay lagoon (a) with a close-up of Qargialuk - Catton Point, where short core position PB is located (b), the southeast side of Qikiqtaruk - Herschel Island, where the position of marine short core HB is located (c) and a close-up of the eastern tip of the island (d), which provides large amounts of sediments due to high cliffs. Locations of panel b and are indicated with yellow rectangles in panel a and c, respectively. Background imagery for insets c,d: Pléiades satellite image acquired on 24 August 2018 (© CNES/Airbus Defence and Space). Background image for inset a, b: GeoEye-1 satellite image acquired on 18 July 2011 (© GeoEye Inc., 2011.).

3.2 Surface water turbidity

The regional surface water temperature and turbidity patterns were driven by the two main wind directions north-northwest (NNW) and east-south-east (ESE) (Fig. 3). During NW-wind conditions cold water from offshore was pushed towards the coast where

https://doi.org/10.5194/egusphere-2026-2314
Preprint. Discussion started: 22 June 2026

surface water temperatures in the lagoon were relatively low (~3°C), and similar to the open ocean (~5°C). The turbidity was also relatively low with ~8 FNU and only slightly elevated compared to the open ocean (~5 FNU) (Fig. 3a). Under ESE-wind conditions this pattern changed drastically (Fig 3b). ESE-winds promoted the influx of warmer waters from the Mackenzie River Plume and lowered the sea level by pushing water offshore. The surface temperatures in the lagoon were higher (~7-8°C) and turbidity was much higher than the open ocean, particularly in the western part of the lagoon with up to 65 FNU. The eastern part of the lagoon, which is sheltered from an inner-lagoon spit, had a relatively low turbidity (~8 FNU), which is comparable to values observed under NW-wind conditions. Following the coast offshore, turbidity remained relatively high in the immediate coastal waters (up to 80 FNU) and decreased swiftly towards the open ocean to ~6 FNU. In comparison to Kanivaliuraq lagoon which is still connected to the ocean, turbidity in the nearby closed lagoon of Whale Bay were nearly unaffected by changing wind direction with turbidity being constantly low (~6-8 FNU). Within the large semi-open river lagoons west of the study area, turbidity was also affected by wind directions (Fig. 3c), particularly under ESE-winds during which turbidity increased along the gravel spits and the shoreline.

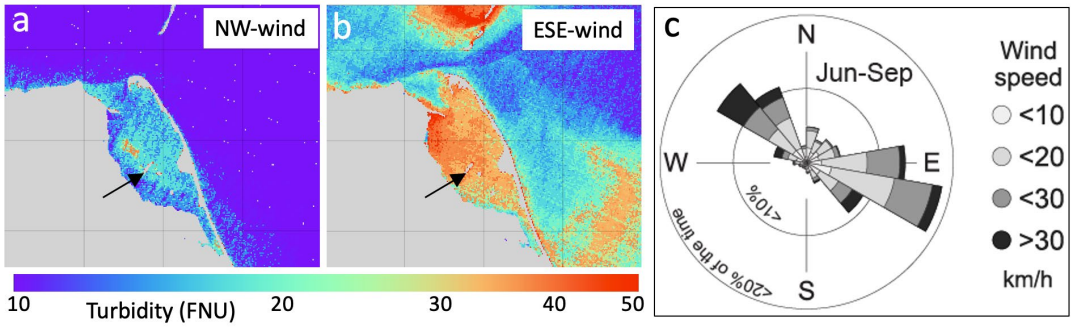

Fig. 3. Map showing surface turbidity (uncalibrated) under prevailing (a) NW and (b) ESE wind directions for the study area Kanivaliuraq – Ptarmigan Bay. Other lagoon systems along the Yukon coast such as Whale Bay (east of Kanivaliuraq – Ptarmigan Bay) and the Firth and Malcolm River barrier lagoons (Figure A4) are displayed as reference. The black arrow indicates the position of an inner-lagoonal barrier, which is situated ~2 km from the inlet and limits sediment input into the enclosed part, where lagoon surface sediments and short cores were taken (see Fig. A1 and Fig. A2). (c) Wind-rose diagram for the study area.

3.3 Radioisotope chronology, mass accumulation and organic carbon accumulation

Short Core Kanivaliuraq - Ptarmigan Bay (PB)

The total ^{210}Pb ($^{210}Pb_{tot}$) activity in lagoon core PB steadily decreased from 62.9 ± 4.1 Bq kg^{-1} at 7 cm to 32.6 ± 2.3 Bq kg^{-1} at ~42 cm depth (Fig. A4), and further to a minimum of 15.8 ± 1.3 Bq kg^{-1} at 53 cm. Activity of ^{226}Ra decreased similarly downcore from 27.7 ± 3.2 Bq kg^{-1} at 5 cm depth to a minimum of 18.2 ± 2.5 Bq kg^{-1} at 52 cm depth, indicative of differences in sedimentary matrix and mineral composition (see also Fig. A3). Activity of ^{137}Cs showed a consistent increase from 2.5 ± 0.4 Bq kg^{-1} (~36 cm) to a 1963 CE peak at ~39 cm (9.5 ± 0.7 Bq kg^{-1}), declining to zero around 46 cm (pre-1950 CE). $Ln^{210}Pb_{ex}$ fits well in the CFCS model (r = 0.93, Fig. A3). Missing $ln^{210}Pb_{ex}$ inventory was inferred from the ^{137}Cs peak, yielding a total inventory of 6001 ± 231 Bq m^{-2} and a flux of 187 ± 7 Bq m^{-2} yr^{-1}. The Constant Flux - Constant Sedimentation (CFCS) model was performed applying Monte Carlo uncertainty for mass accumulation rate (MAR) and sedimentation rate (SR; Fig. A5). Since the 1950s, mass accumulation rates (MAR) and OC mass accumulation rates (OC_{MAR}) have increased markedly (Table 1). MAR rose from 0.32 ± 0.05 g cm^{-2} yr^{-1} (1953-1972 CE) to 0.57 ± 0.05 g cm^{-2} yr^{-1} (1972-2011 CE), and 0.57 ± 0.09 g cm^{-2} yr^{-1} in recent times (2011-2018 CE).

https://doi.org/10.5194/egusphere-2026-2314
Preprint. Discussion started: 22 June 2026

OC_{MAR} followed a similar trend: increasing from 0.24 ± 0.07 kg m^{-2} yr^{-1} (1953-1972 CE) to 0.48 ± 0.08 kg m^{-2} yr^{-1} (1972-2011) and 0.39 ± 0.05 kg m^{-2} yr^{-1} (2011-2018 CE), respectively (Table 1).

Short Core Herschel Basin (HB)

The total ^{210}Pb ($^{210}Pb_{tot}$) activity in marine core HB varied between 34–48 Bq kg^{-1} in the top 10 cm (Fig. A4). Below 15 cm, it declined from 49.3 ± 3.1 to 35.7 ± 2.2 Bq kg^{-1}. Activity of ^{226}Ra was stable (26.7 ± 0.8 Bq kg^{-1}, n = 11), consistent with constant grain size, mineralogy, and TOC (Fig. A3). Although activity of ^{137}Cs was lower and pre-1950s not reached, its rise from 0.9 ± 0.3 Bq kg^{-1} (2 cm) to a maximum of 3.8 ± 0.4 Bq kg^{-1} (38 cm) suggests the 1963 CE peak was captured, followed by a decline towards core bottom (*Falardeau et al., 2023b*). $ln^{210}Pb_{ex}$ from ~11 cm to bottom had a correlation of r = 0.91 (Fig. A3). The estimated missing inventory (~15%) was inferred from ^{137}Cs, resulting in a total inventory of 6755 ± 183 Bq m^{-2} and flux of 210 ± 6 Bq m^{-2} yr^{-1}. The CF model with Monte Carlo simulation was also applied here (Fig. A5). MAR and OC_{MAR} have increased markedly throughout the three periods, 0.57 ± 0.10 kg m^{-2} yr^{-1} (1953-1972 CE) to 0.65 ± 0.11 kg m^{-2} yr^{-1} (1972-2011 CE) and culminating in 1.57 ± 0.56 kg m^{-2} yr^{-1} (2011-2018 CE) (Table 2).

Table 1. Mean mass accumulation rates (MAR) and OC mass accumulation rates (OCMAR) for the Kanivaliuraq lagoon – Ptarmigan Bay (PB) and marine reference site Herschel Basin (HB) for different periods between 1953 and 2018 CE. Periods were chosen to match periods with shoreline change rates. Mean rates are provided with ± standard deviation.

	1953-1972 CE	1972-2011 CE	2011-2018 CE
Lagoon (short core PB)			
MAR (g cm^{-2} yr^{-1})	0.32 ± 0.05	0.57 ± 0.05	0.57 ± 0.09
OCMAR (kg m^{-2} yr^{-1})	0.24 ± 0.07	0.48 ± 0.08	0.39 ± 0.05
Marine (short core HB)			
MAR (g cm^{-2} yr^{-1})	0.57 ± 0.10	0.65 ± 0.11	1.57 ± 0.56
OCMAR (kg m^{-2} yr^{-1})	0.07 ± 0.03	0.13 ± 0.03	0.40 ± 0.18

3.4 Sediment Characteristics and Geochemistry

Kanivaliuraq - Ptarmigan Bay Core (PB) shows a heterogeneous matrix with distinct vertical sections (Fig. A3). The upper section (0-35 cm) was composed of fine-grained, laminated sediment with low bulk density (~0.7 ± 0.1 g cm^3), high TOC (7.5 ± 2.2 wt%), TOC/TN of 15.5 ± 1.0, and $\delta^{13}C$ of -27.0 ± 0.2‰. The middle section (35-55 cm) was composed of coarser sediments with more sand, higher density (~1.1 ± 0.1 g cm^3), and lower TOC (4.6 ± 1.2 wt%). TOC/TN increases (19.2 ± 2.1), and $\delta^{13}C$ remains -27.0 ± 0.02‰. The lower section (55-64 cm) until the core bottom was composed of dark, fine-grained sediment with high TOC (17.4 ± 0.4 wt%, max 26.5 wt%), high TOC/TN (19.0 ± 0.7), and $\delta^{13}C$ of -27.2 ± 0.2‰.

Short Core 1 (Stream Outlet) exhibited high TOC (13.1 ± 4.9 wt%) and TOC/TN (21.8 ± 2.7), with consistently low $\delta^{13}C$ (-28.4 ± 0.1‰) (Fig. 6). Downcore, TOC and TOC/TN vary, with lowest values (~5 wt%, TOC/TN ~16.7) at depths containing most sand (~26.6%).

https://doi.org/10.5194/egusphere-2026-2314
Preprint. Discussion started: 22 June 2026

Short Core 2 (Central Lagoon) showed relatively low TOC (2.8–6.3 wt%), but TOC/TN ratios remained high (22.2 ± 1.8) and $\delta^{13}C$ was -27.3 ± 0.1‰ (Fig. 6). Like core 1, lowest TOC values aligned with sandy layers (~20 cm depth).

Marine Short Core (Herschel Basin - HB) showed a more homogeneous, fine-grained matrix and higher density (1.0 ± 0.1 g/cm³) (Fig. A3). TOC and TOC/TN were lower than lagoon cores (values not fully given; TOC/TN: 12.7 ± 1.6). $\delta^{13}C$ (-26.3 ± 0.2‰) is higher than in PB. A shift in sediment structure and grain size occurred at ~9 cm. The upper section was sandier (15.9 ± 6.6%) and laminated; the lower section was finer (8.3 ± 2.3%). Marine core HB was chemically distinct, with lower TOC and higher $\delta^{13}C$, reflecting marine OM input.

Lagoon surface sediments reflected the transition from terrestrial sources to more offshore samples (Fig. 4). Near the stream outlet we observed high TOC (13.1 ± 4.9 wt%), TOC/TN (21.8 ± 2.7), and low $\delta^{13}C$ (-28.3 ± 0.1‰), which closely resembled nearby permafrost and active layer values. $\delta^{13}C$ values were lowest near the outlet in both vertical and lateral data. Inland permafrost showed high TOC (~19.9 ± 8.7 wt%), and moderate TOC/TN (~19.6). Further from the outlet (short core 2), TOC declined (5.3 ± 0.9 wt%), $\delta^{13}C$ rose (-27.3 ± 0.1‰), while TOC/TN remained stable (22.2 ± 1.8). Marine sediments showed the lowest TOC (1.7 ± 0.2 wt%) and TOC/TN (12.8 ± 1.4), and highest $\delta^{13}C$ (-26.2 ± 0.2‰). TOC and OC loading decreased sharply with distance from the outlet. OC loading correlated strongly with TOC (R^2 = 0.8), but not with $\delta^{13}C$ or sand volume. $\delta^{13}C$ increased gradually (-27.8 to -27.4‰) and TOC/TN slightly decreased (19.6 to 16.5). Sand content increased toward the central lagoon, peaking at 21%, but was absent in protected distal locations. Downcore and lateral trends showed consistent TOC depletion and $\delta^{13}C$ enrichment away from inland permafrost.

Table 2. Organic carbon and nitrogen pools for the upper 30 cm in the terrestrial catchment and in lagoon sediments of the Kanivaliuraq lagoon – Ptarmigan Bay (PB), as well as in marine Herschel Basin. Terrestrial pools are from Wagner et al. (2023). PB (lagoon) and HB (marine) data are based on averages and standard deviations from the upper 30 cm in lagoon and marine sediment cores, respectively. A consistent depth interval was chosen, which is limited by marine sediment core depth for better comparability of the data.

	Organic carbon pool ($kg\ m^{-2}$)	Nitrogen pool ($kg\ m^{-2}$)
Terrestrial	23.2 ± 3.31	1.3 ± 0.24
Lagoon	14.1 ± 4.54	1.12 ± 0.39
Marine	7.5 ± 1.33	0.69 ± 0.07

https://doi.org/10.5194/egusphere-2026-2314
Preprint. Discussion started: 22 June 2026

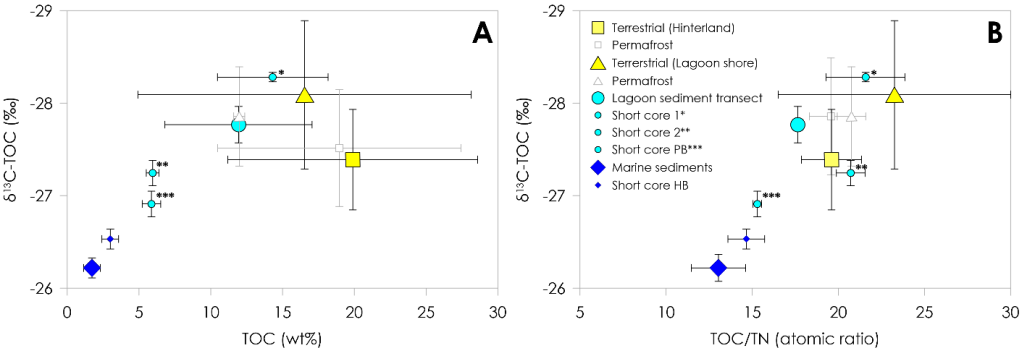

Fig. 4. Scatter plots displaying TOC contents (A) and TOC/TN-ratios (B) against δ13C-TOC values for terrestrial, lagoon and marine sediment samples. From the lagoon and marine short cores, only the upper 5 cm were used and displayed here as surface sediments corresponding to the lagoon surface samples, which were taken with a Van-veen grab sampler covering the upper ~5-6 cm of sediment. The asterisk (*) indicates the position of short core 1 (Stream outlet/mudflat), two asterisks (**) the location of short 2 (Central) and three asterisks (***) the location of short core Kanivaliuraq - Ptarmigan Bay (PB). Short core 1 (Stream outlet/mudflat) was taken at the enclosed end of the lagoon, where a small stream drains into the lagoon. The marine short core HB was taken on the slope of Herschel Basin.

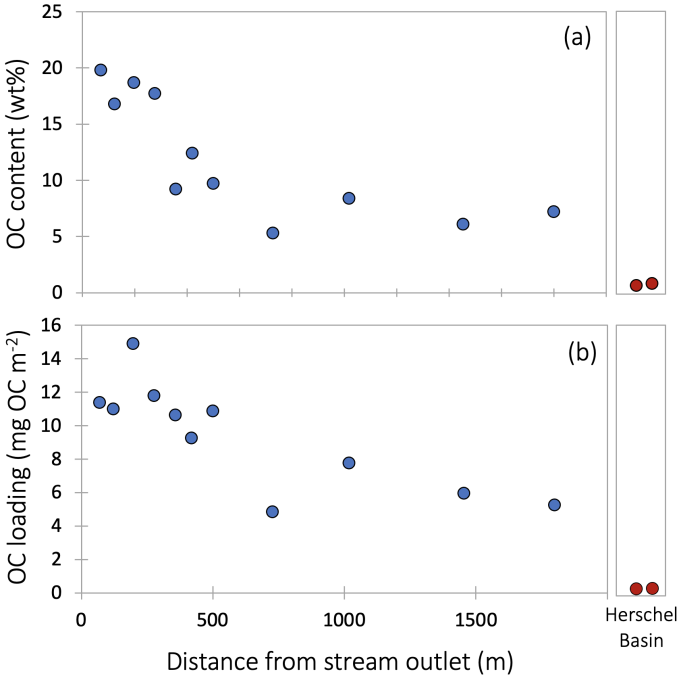

Fig. 5. Organic carbon content (a) and OC mineral surface area loading (b) in wt% and mg m^{-2}, respectively, along a ~2 km sampling transect of surface sediments from the enclosed part (stream outlet location) to the central part of the lagoon. Blue circles are data from this paper, red circles are from Jong et al. (2024) from further outside the lagoon off shore in Herschel Basin at water depths of 20 and 37m.

https://doi.org/10.5194/egusphere-2026-2314
Preprint. Discussion started: 22 June 2026

365

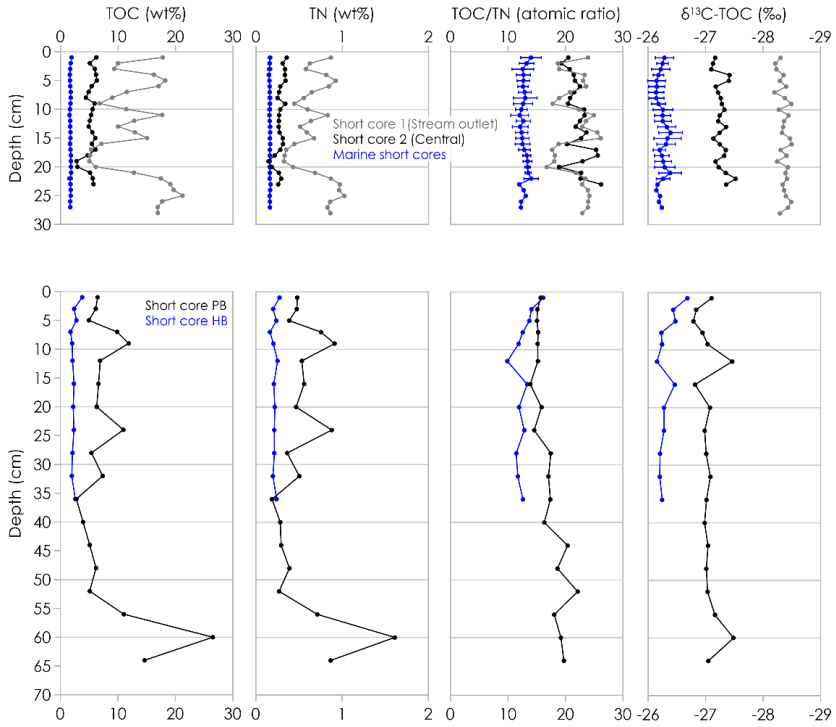

Fig. 6. Scatter plots showing TOC and TN contents, TOC/TN-ratios as well as δ13C-TOC values for short core 2 (Stream outlet), short core 1 (Central) and the marine short cores compilation in the upper panels. Data for short core Kanivaliuraq - Ptarmigan Bay (PB) and short core Herschel Basin (HB) are displayed separately in the lower panels for better visualisation.

370

3.5 Shoreline and lagoon size changes over time

Between 1953 and 1972, shoreline retreat at Kanivaliuraq Lagoon averaged −0.6 ± 0.8 m yr^{-1}, leading to a total lagoon expansion of 70,666 m^2 which translates into an annual area loss of 3,926 m^2 yr^{-1}. This erosion delivered 3,425 t of organic carbon (OC), which converts to an annual OC flux of 190 t yr-1 (Table 3, Fig. 7). From 1972 to 2011, retreat rates slightly increased to −0.9 ± 0.8 m yr^{-1}, with an area of 159,431 m^2 being eroded (4,088 m^2 yr-1) and 7,568 t of OC export and an OC flux of 194 t yr^{-1} (Table 3). The most recent period 2011–2018 shows a marked acceleration in erosion to −3.3 ± 0.7 m yr^{-1}, which resulted in the erosion of 188,832 m^2 causing an OC export of 9,323 t OC flux. This converts into an annual OC flux of 1,332 t yr^{-1} (Table 3).

375

https://doi.org/10.5194/egusphere-2026-2314
Preprint. Discussion started: 22 June 2026

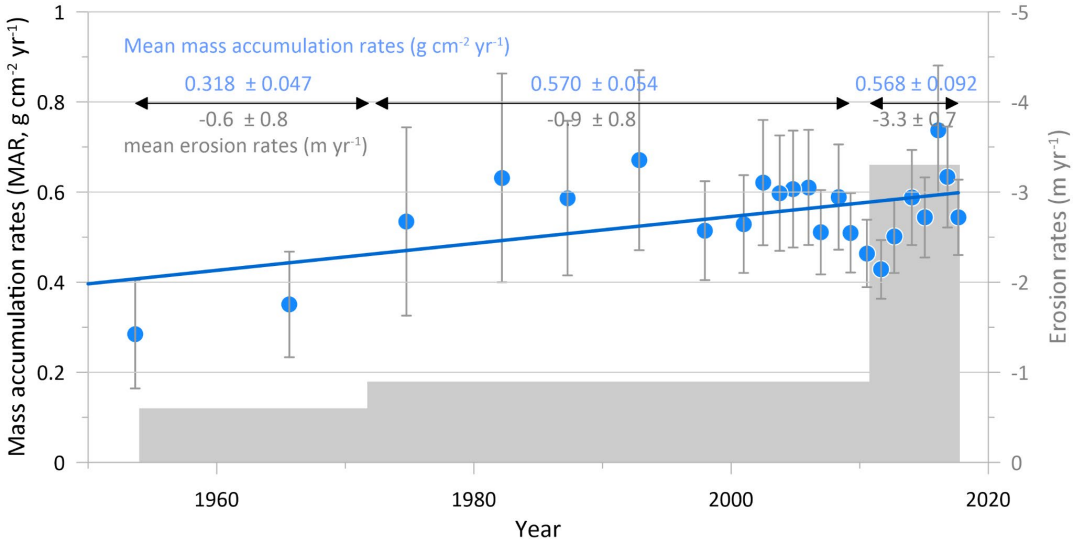

Fig. 7. Mass accumulation rates (MAR) and coastal erosion rates for the lagoon system Kanivaliuraq – Ptarmigan Bay lagoon over time (1953-2018 CE). Error bars are Monte Carlo simulation uncertainties. Grey bars show erosion rates for the three time windows. The linear regression ($R^2 = 0.26$; $p = 0.013$; $n = 23$) outlines the trend for the mass accumulation rates.

Table 3. Summary of shoreline change rates, lagoon area changes and related OC fluxes for the Kanivaliuraq lagoon for different periods between 1953 and 2018 CE.

Period	Shoreline change rate (m yr^{-1})	Eroded area = lagoon growth (m^2)	Annual area loss (m^2 yr^{-1})	OC export into lagoon (t)	Annual OC flux (t yr^{-1})
1953-1972 CE	-0.6 ± 0.8	70,666	3,926	3,425	190
1972-2011 CE	-0.9 ± 0.8	159,431	4,088	7,568	194
2011-2018 CE	-3.3 ± 0.7	188,832	26,976	9,323	1,332

4. Discussion

4.1 Increasing erosion rates are reflected in sediment accumulation rates

Kanivaliuraq lagoon is subject to substantial erosion, which mobilises sediment and OM from land. The majority of the inner-lagoon shoreline (~70%) is characterized by strong erosion with mean rates of 3.3 ± 0.7 m yr^{-1} and extremes of up to 21.7 m yr^{-1} (2011-2018; Table A2 and Fig. 2a), comparable to other strongly erosive sites in the area with up to -22.0 m yr^{-1} (Obu et al., 2017; Irrgang et al., 2018). The high erosion rates make Kanivaliuraq lagoon a hotspot for coastal erosion in the western Canadian Arctic. The intense shoreline change in the lagoon is most likely primed by inundation of lowlying tundra and the erosion of low cliffs. Low water levels and negative surges that prevail particularly under SE-winds conditions during almost half the summer season (June to September) (Héquette and Barnes, 1990; Héquette et al., 1995) lead to frequent resuspension and transport of sediment within the lagoon. Although the inner-lagoon barrier spit (Figs. 1b, A2) may block transport of suspended sediments, eroded material likely reaches the enclosed part of the lagoon as the general direction of the current (i.e., in Workboat Passage; Fig. 1a) is from northwest to southeast. The direction of currents is indicated by the recurving of the spit at the inlet of the lagoon and by

https://doi.org/10.5194/egusphere-2026-2314
Preprint. Discussion started: 22 June 2026

various smaller spits within the lagoon (Pelletier, 1987; Fig. A2). In contrast to that, outside of the lagoon sediment is transported from east to west along the Yukon coastline (Forbes, 1997) and in southerly directions along the eastern coastline of Qikiqtaruk (Fig. 2c) towards the lagoon (Pelletier and Medioli, 2014). The high bluffs towards the east of the lagoon and along the southeast coast of Qikiqtaruk (Fig. 2d) may therefore be additional sources of OM and sediment into the lagoon.

Sedimentation rates in Kanivaliuraq lagoon increased from the 1950s until recent years (i.e., 2018 CE), corresponding to the increasing erosion rates in the same period (Fig. 7). In the last decade of observation (2011-2018 CE), apparent erosion rates increased by a factor of four compared to 1970-2011 CE. While an annual relationship cannot be established due to a lack of high-resolution satellite images (to resolve annual shoreline changes), the sedimentation rates from short core PB seem to be related to the observed erosion rates. Short core PB was collected from a depocenter (basin with high accumulation rates), sheltered from strong currents and wave-induced resuspension, which is indicated by the fine lamination in the core, particularly in the upper section (~0-35 cm) and a continuous, undisturbed sedimentation. Depocenters are typical for lagoons and form between corridors of strong currents (Schreiner et al., 2013). Within the core, coarser grain size (~35-55 cm) may indicate spit overwash events and sand relocation in the 1950s-1960s (Fig. A3) and relatively high TOC contents in the bottom section (~55-65 cm) potentially relate either to an increasing inflow of terrestrial OC or inundated tundra with high OC content.

Sedimentation rates in the marine reference short core HB increased by a factor of more than two in the last decade (Fig. A5), likely caused by erosion and sediment supply from Qikiqatruk and the Yukon Coastal Plain (Obu et al., 2016, 2017, 2017; Couture et al., 2018, Grotheer et al., 2020). Yet, the mean erosion on the southeast side of Qikiqatruk did not change much over time (0.8 m yr^{-1} in 1972-2011 CE and 0.7 m yr^{-1} in 2011-2018 CE), suggesting either an additional sediment supply from other sources such as erosion of the Yukon mainland (Couture et al., 2018). The sedimentation rates are particularly high in the last decade with high deposition and potential reworking of sediments (Fig. A3) particularly visible in the upper section (~0-10 cm), and less so in deeper layers (~10-38 cm). The C/N ratios and $\delta^{13}C$ values suggest arrival and burial of terrestrial OM (Naidu et al., 2000; Grotheer et al., 2020). Additional sediment input can be derived from the Mackenzie River, which has shown an increase in discharge and sediment supply during the last decades (Doxaran et al. 2015; Tank et al., 2016). Strong SE winds, which are more frequent after 1998 CE (Falardeau et al., 2023b) would favour the spreading of the particle-rich Mackenzie River plume towards Herschel Basin. Other possible sources could be the Babbage River or retrogressive thaw slump systems, which are widespread along the Yukon coast and increased in size and activity during the last decades (Ramage et al., 2018). The increase in erosion rates and sedimentation rates in both lagoon and marine environments may reflect the generally observed accelerated environmental changes in the Arctic coastal zone (Fritz et al., 2017; Irrgang et al., 2022; Nielsen et al., 2022; Falardeau et al., 2023a) as well as intensified permafrost degradation in the hinterland priming erosion process (Angelopoulos et al., 2021, Creel et al., 2024).

4.2 Transformation of organic matter along the land-lagoon-ocean gradient

Sedimentary OM characteristics gradually change from land via the shallow parts (<1 m water depth) towards the deeper channel of the lagoon (>2 m water depth) and ultimately into the marine environment. Lagoon sediments close to shore (short core 1) reflect the OM characteristics of terrestrial sediments with relatively high TOC contents and TOC/TN-ratios (13.1 ± 4.9 wt% and 21.8 ± 2.7, respectively) and low $\delta^{13}C$ values (-28.4 ± 0.1 ‰) (Fig. 6). The terrestrial fingerprint of lagoon sediments suggests that large portions of terrestrial OM were deposited right away in the lagoon due to erosion or inundation, which is a typical process along the low-lying coastal parts of the Yukon Coastal Plain and lagoons (Forbes, 1997; Irrgang et al., 2018). The input of

https://doi.org/10.5194/egusphere-2026-2314
Preprint. Discussion started: 22 June 2026

suspended fluvial OM from the stream is low as the majority of the fluvial OM is composed of dissolved organic carbon (DOC) (Speetjens et al., 2022), similar to other low-relief streams in the study area (Coch et al., 2018, 2019). Yet, pronounced stream water inflow during the spring freshet or rain/storm events may rework parts of the eroded material at the lagoon rim (Speetjens et al., 2022) and increase the input of POC.

The strong decrease in TOC content and OC loading in combination with ^{13}C enrichment towards the central part of the lagoon (Fig. 4a and Fig. 5) suggests active OM degradation and/or leaching processes (Weiss and Kaal, 2018) during lagoon transport. Although it has to be noted that the ^{13}C enrichment could also be caused by the dilution with marine material (Naidu et al., 2000; Tanski et al., 2017). Benthic microalgae (Schreiner et al., 2013) as well as ice algae and phytoplankton (Dunton et al., 2006) can contribute to the sediment OC pool in lagoons, and, especially during NW-winds, seawater masses could deliver additional marine-derived OM. From the central part of the lagoon towards the sediments of Herschel Basin, the OM contents decrease further (Fig. 5a). In contrast to the lagoon sediments, TOC contents in the marine sediments are less variable but maintain a terrestrial signature as indicated by $\delta^{13}C$ values (-26.2 ± 0.2‰) and TOC/TN-ratios (12.8 ± 1.4). Most of the OM (up to 90%) is derived from terrestrial sources and most likely from coastal erosion and fluvial material, with a marginal marine autochthonous OM component (Couture et al., 2018; Grotheer et al., 2020).

Towards the central part of the lagoon, OM content significantly decreases from 13.1 ± 4.9 wt% (short core 1) to 6.0 ± 0.4 wt% (short core 2) (Fig. 4a). The decreasing OC content goes hand in hand with a strong decrease in OC loading (values above 14 mg OC m^{-2} to around 4-6 mg OC m^{-2}). These values are much higher than in typical estuarine or riverine settings Keil et al., 1997; Aller and Blair 2006) likely due to the presence of so-called matrix-free OC (vegetation debris, plant remains) that is abundantly released via coastal erosion in the Beaufort Sea (Van Crimpen et al., 2024). This material is not bound to minerals so essentially masks the reliable interpretation of spatial patterns of OC loading. However, mineral OC loading in offshore marine settings is much lower, with 0.68 ± 0.23 mg OC m^{-2} around Herschel Island (bulk samples, Jong et al., 2020) and 0.45 mg OC m^{-2} in Herschel Basin (high-density fine fraction; Jong et al., 2024; Fig. 5). This suggests a loss of mineral-bound OC during transport and/or a relative decrease in the amount of matrix-free OC, for example via consumption by marine fauna grazing within the lagoon (Dunton et al., 2006). At the same time, the sand fraction increases within the channel towards the central part of the lagoon (up to 21.2 vol.%) where OC content and loading is also lowest. The increase of sand fractions indicates the removal of light and fine-grained OC-bearing particles by strong currents in the channel through winnowing, resuspension, and offshore transport (Jong et al., 2020; Radosavljevic et al., 2022).

Various water column and sedimentary processes within lagoon systems can favour degradation of OM. In general, summer water temperatures in lagoons may be higher than marine systems facilitating OC turnover by microbes (Lee et al., 2012). In the Kanivaliuraq-Ptarmigan lagoon this is mostly driven by wind direction, with higher temperatures (~7-8°C) during SE wind conditions, and NW winds favouring the inflow of cold water masses into the lagoon (~5°C to ~3°C). Yet, the influx of seawater could promote priming effects and co-metabolization of OM (Bianchi, 2011). In summer, high nutrient contents and small particle sizes along the lagoon's rim may support the abundance of chemoorganotrophic bacteria, which are specialised in degrading OM (Zhang et al., 2013). In the upper sediment column sufficient oxygen may be available for aerobic respiration of OM, although low temperatures limit the CO_2 production rates (Arndt et al., 2013; Knoblauch et al., 2013). For similar lagoons along the Beaufort Sea, it was shown that lagoons are episodic sources of CO_2, which are driven by carbonate thermodynamics, precipitation of ikaite, and the supply of sediments complementing the OM degradation and respiration of CO_2 (Miller et al., 2021).

https://doi.org/10.5194/egusphere-2026-2314
Preprint. Discussion started: 22 June 2026

In winter, most of the lagoon (in 2017 this was 75%, Angelopoulos et al., 2020a) is covered with bedfast ice, i.e., a completely frozen water column because average water depths are smaller than the local thickness of sea ice (Solomon et al., 2000). Since lagoon sediments may freeze during bedfast ice conditions, depending on the salinity of the sediments, OM turnover may get significantly reduced during the cold season (Jenrich et al., 2021) although OM degradation and production of CO_2 by respiration may proceed under sub-zero conditions (Mackelprang et al., 2011; Natali et al., 2019). We suspect most degradation of sedimentary OC will take place during the open water season.

4.3 Enhanced organic matter sequestration in lagoon sediments

The semi-open Kanivaliuraq lagoon shows higher OM pools than nearshore marine sediments (Table 2, Fig. 5a). Although MAR is similar for both systems (Table 1) with exception of the most recent observation period (2011-2018), the higher OM contents in the lagoon suggest a higher total accumulation of OM in the lagoon compared to the marine sediments. The TOC pools in the lagoon short core PB (0 - 30 cm depth, 14.1 ± 4.54 kg m^{-2}) are almost twice as high as in the marine short core HB (7.50 ± 1.33 kg m^{-2}), indicating greater OM sequestration in sheltered parts of lagoons compared to nearshore sediments. The OC pool in the lagoon is larger than OC pools observed in other regions such as Siberia, where OC pools in the upper 3 m of thermokarst lagoons range from 22.5 to 26.5 kg m^{-2} (Jenrich et al., 2021) and on Richards Island in the Mackenzie Delta with 25 kg m^{-2} (Solomon et al., 2000). Yet it has to be noted that depth intervals vary for both studies. A study by Grotheer et al. (2020) on a 12.3 m long marine sediment core in Herschel Basin shows constant TOC contents (1.8 ± 0.1 wt%) over the last centuries, which are almost similar to the TOC contents in the other short marine sediment cores (1.7 ± 0.2 wt% (Grotheer et al., 2019)), yet lower than in marine short core HB (2.4 ± 0.5 wt%). This might be caused by preferential settling of terrestrial OM from erosion close to shore (Tanski et al., 2017; Angelopoulos et al., 2020; Jong et al., 2020). Assuming a homogeneous dry bulk density of marine sediments in Herschel Basin, the lower TOC contents of most marine sediments (Tanski et al., 2017; Grotheer et al., 2019, 2020; Jong et al., 2020, this study) would result in a lower TOC pool as inferred from marine short core HB (Table 2). This emphasizes the OM burial capacity of lagoons, which is about two times higher than in nearshore marine sediments.

Terrestrial OC pools in the nearby hinterland (23.2 ± 3.31 kg m^{-2}; Table 2) are higher than in the Kanivaliuraq lagoon, emphasizing the stepwise transition and degradation of OC from land to lagoon to marine settings. This transition is supported by an overall shift from terrestrial towards a lacustrine/marine TOC/TN-ratio and $\delta^{13}C$ signature, but also efficient long-term deposition in the lagoon. For the inundated lagoon shoreline sections, we expect even higher OM burial potential since it directly fringes wet-polygonal tundra with large stocks of permafrost carbon, possibly delivering further OM with further shoreline erosion or inundation (Jenrich et al., 2021). The general trend of increasing erosion in the Arctic in combination with warmer temperatures triggering thermokarst lagoon development may catalyse sedimentation and effective carbon burial in lagoons and thus long-term sequestration of carbon (Jenrich et al., 2021, 2025).

4.4 Widespread spatial extent of lagoon system along the Beaufort Sea

Lagoon systems intercept and potentially influence OM characteristics substantially along large parts of the coastline in the western Canadian Arctic and Alaska. Whereas semi-open lagoon systems such as Kanivaliuraq lagoon make up only a minor portion (~5%) of the Yukon's Arctic coastline, river lagoons make up approximately ~20% of the coastline in our study area. In these systems

https://doi.org/10.5194/egusphere-2026-2314
Preprint. Discussion started: 22 June 2026

the terrestrial input is dominated by fluvial OM input (Schreiner et al., 2013). Especially in short distance to the river mouth most of the OM is of fluvial origin derived from the coastal hinterland, OM sources come from plants and soils inland or from in situ production within the stream network itself (Magen et al., 2010). Yet, as in semi-open lagoons terrestrial OM input from shoreline erosion could be a significant contributor and even dominate when outside of the main river plume and in the enclosed parts of riverine lagoons nestled between shores (Schreiner et al., 2013). East to the Yukon coast semi-open lagoons, which are similar to Kanivaliuraq lagoon, are present along Richards Island or the Tuktoyaktuk Peninsula. Here, the coast is dominated by thermokarst lakes that transform into lagoons once breached by shoreline retreat (Solomon et al., 2000). Whereas the Mackenzie River contributes substantially to the OM input of lagoons on Richards Island and the western part of the Tuktoyaktuk Peninsula due to its massive inflow of suspended particles to the coastal waters, the terrestrial OM supply of the lagoons further to the east of Tuktoyaktuk is dominated by lacustrine deposits, shoreline erosion or marine in situ production (Lavoie et al. 2009). To the west of the Yukon-Alaskan border, large river lagoons dominate the Alaskan coastline of the Beaufort Sea (Jorgenson and Brown, 2005). Yet, various smaller lagoons and semi-open lagoons similar to Kanivaliuraq lagoon exist, which have smaller streams draining into the lagoon and are protected by barrier spits with the lagoon only connected via relatively narrow channels to the open ocean. Examples from the Alaskan Beaufort coast are the lagoons of Kaktovik, Nuvagapak, Demarcation Bay (Harris et al., 2018), Elson lagoon, Cape Halkett (Jones et al., 2009) and Simpson lagoon (Dunton et al., 2006; Schreiner et al., 2013; Hanna et al., 2014). Pogik Bay or Mikkelsen lagoon may resemble similar OM deposition regimes as Kanivaliuraq lagoon with coastal erosion being the main OM source and the sheltered setting favouring long-term deposition of large OM pools compared to nearshore marine sediments (Goñi et al., 2000; Naidu et al., 2000).

4.5 Broader implications of lagoons as reactors in the Arctic nearshore zone

Arctic permafrost lagoons and embayments may have profound implications on the Arctic carbon cycle and ecosystems, especially under the current rapid environmental changes. Almost one third of the Yukon coast and major parts of the western Canadian are affected by lagoon systems (This study, Jenrich et al. 2025b, 2025c, Couture et al., 2018), which are similarly ubiquitous along Alaskan and Siberian coasts (Jenrich et al., 2025c; Dunton et al, 2006; Krylenko et al., 2017). In combination with the observed rapidly changing environmental conditions that promote enhanced OM transfer from land to sea such as proceeding permafrost degradation, increased coastal erosion, warming air and sea temperatures, these systems play a crucial role as receptors and reactors of OM on transit from land to sea, potentially on a magnitude similar to Arctic nearshore zones (Fritz et al., 2017), river estuaries (Clark et al., 2022) or fjord systems (Bianchi et al., 2020). The emerging role of lagoons as OM reactors along the land-ocean boundary is in line with the concept of Aquatic Critical Zones (ACZs, e.g., Bianchi et al., 2020), which may offer a transferable framework for Arctic permafrost-dominated shelves by emphasizing the tight coupling of physical forcing, sediment dynamics, and OM transformation across the land–ocean interface. From this perspective, nearshore zones act as dynamic biogeochemical reactors where mobilized permafrost-derived OM is selectively degraded, reworked, or preserved before export to the open shelf. Yet, more research is needed to differentiate various lagoon types and embayments and link environmental drivers to lateral and vertical OM fluxes within these systems and address their role for the Arctic carbon budget and local ecosystems. For instance, lagoon systems that receive large amounts of permafrost OM may be underestimated vents for greenhouse gases, whereas in riverine lagoon systems the interplay of different OM sources may have drastic implications on the actual composition,

https://doi.org/10.5194/egusphere-2026-2314
Preprint. Discussion started: 22 June 2026

bioavailability and pathways of OM. Also, local and regional environmental characteristics need to be considered to better constrain OM transformation processes in lagoon systems including the (seasonal) effects of sea ice coverage, brine formation, phytoplankton blooms, water temperature, oxygen availability, turbidity or microbial characteristics and (co-)metabolization dynamics. Since the pace of coastal erosion is accelerating, research should focus on the role of lagoon systems for OM transfer and transformation and attempt to estimate and model future changes for carbon budgets.

5. Conclusion

Arctic lagoons and embayments are crucial transitional landscapes for OM mobilization, transport, burial and degradation at the interface between land and ocean. Ongoing environmental changes, increasing erosion rates, relative sea level rise and intensified OM transfer from land to sea in the Arctic may enhance the importance of lagoons as geochemical reactors for terrestrial OC. As 'natural reactors' these shallow aquatic systems intercept large amounts of OC between land and shelf, functioning as efficient depocenters for OC burial, yet at the same time have a high potential for venting of greenhouse gases into the atmosphere. Therefore, Arctic lagoons both function as major OC sinks and hotspots for remineralization and primary production. With further accelerating coastal erosion and permafrost degradation along the Arctic coast as a consequence of Arctic warming, we expect increasing OM accumulation and processing in lagoon and embayment systems which will lead to altering carbon pathways in the Arctic. Longer open water seasons and increasing storm frequencies may alter the dynamics of Arctic lagoons and embayments in the future.

https://doi.org/10.5194/egusphere-2026-2314
Preprint. Discussion started: 22 June 2026

Appendices

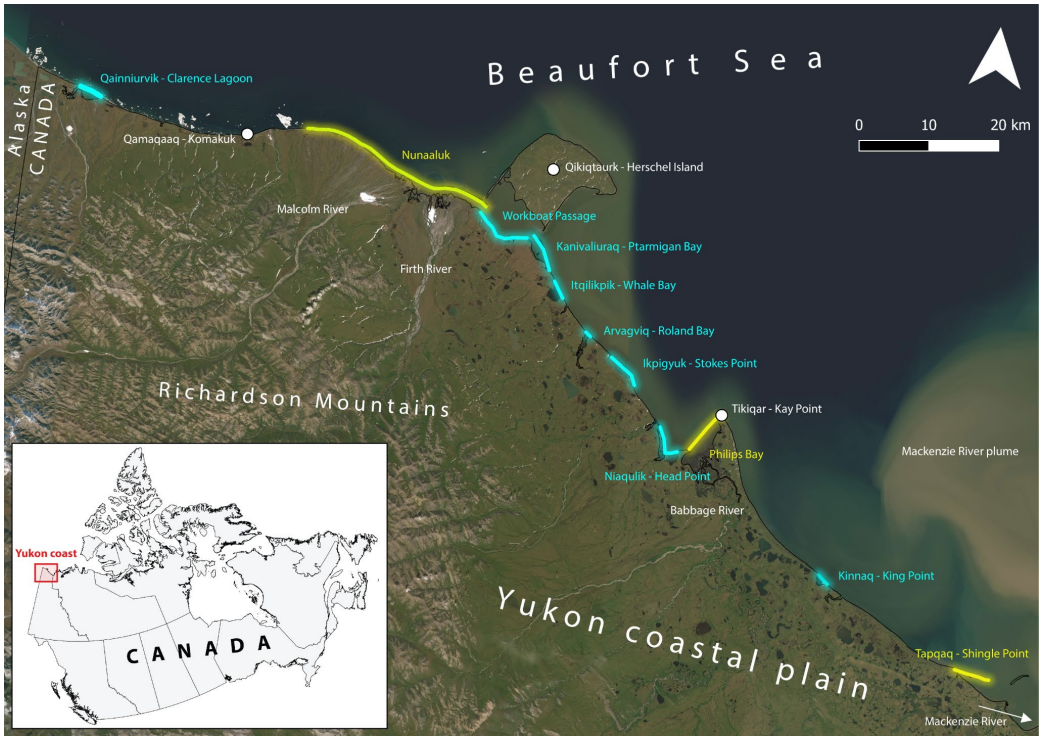

Fig. A1. Map showing the Yukon coast and the location of major spit systems (yellow), as well as lagoons, embayments and bays (blue lines). These systems which are partly or completely cutting water flow to the open ocean characterize approximately 35% of the coastline. Background imagery: Sentinel-2 satellite imagery, RGB composite (Copernicus Programme, European Space Agency), acquired on 27 July 2017.

https://doi.org/10.5194/egusphere-2026-2314
Preprint. Discussion started: 22 June 2026

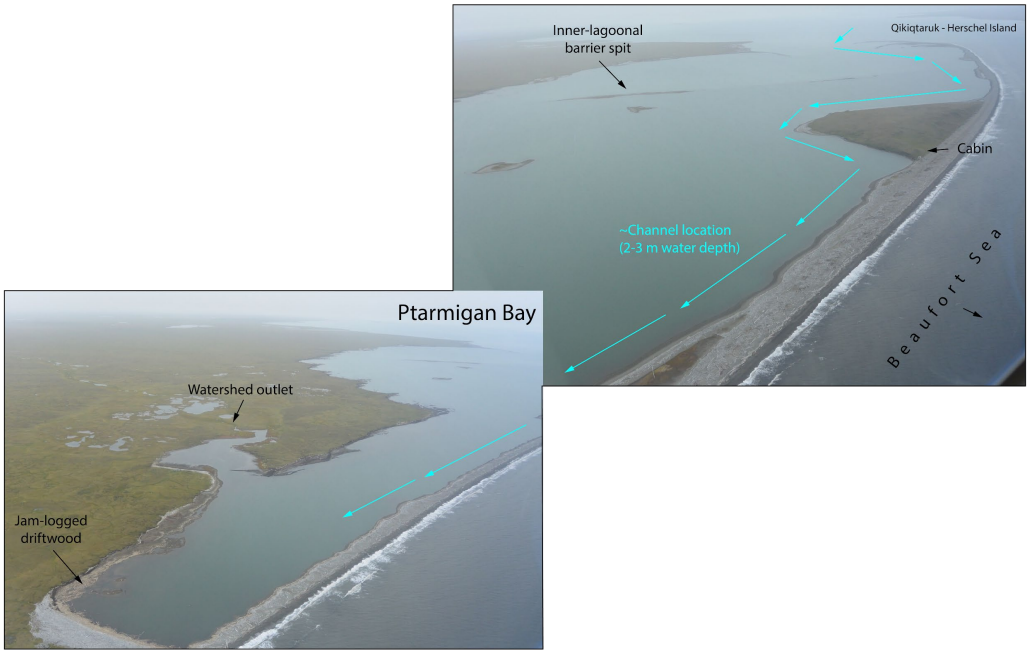

565 **Fig. A2. Oblique airborne photographs of the open lagoon system Kanivaliuraq – Ptarmigan Bay (PB). A gravel spit barrier is protecting the lagoon from the environmental forcing of the open Beaufort Sea. The spit runs in the north-northwest direction and is approximately 6 km in length. In the lagoon, a deeper channel (2-3 m depth) is situated close to the barrier spit. The remainder of the lagoon system is very shallow (<1 m water depth). Herschel Basin (HB) is located north-east of the lagoon and is part of the Beaufort Sea shelf. The blue arrow-line shows the dominant flow direction of the water. Picture credit: G. Tanski and A. Irrgang (2015).**

https://doi.org/10.5194/egusphere-2026-2314
Preprint. Discussion started: 22 June 2026

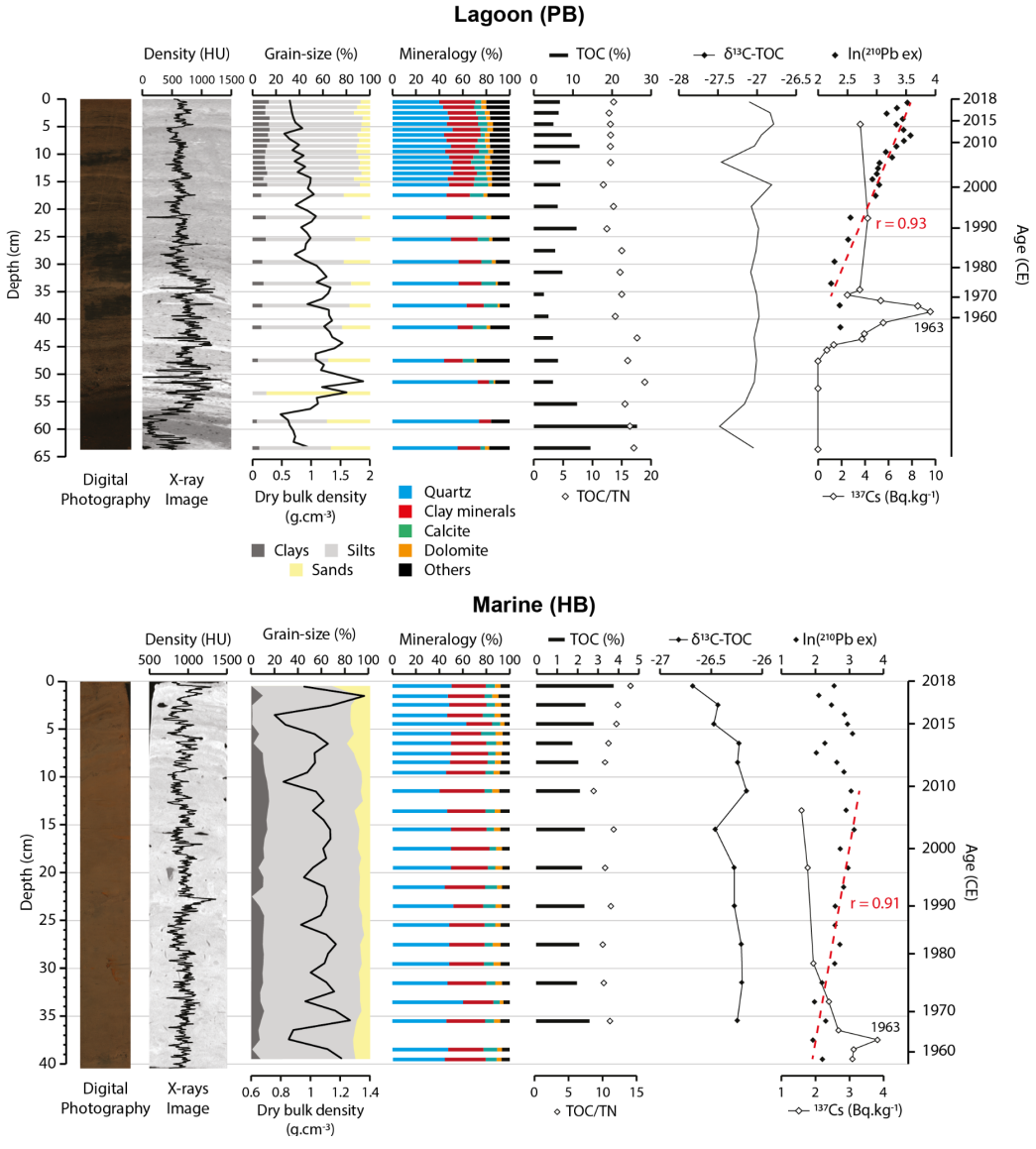

570

Fig. A3. Summary of sedimentological and geochemical data for lagoon short core Ptarmigan Bay (PB) and marine reference short core Herschel Basin (HB). Red dashed lines indicate regression lines.

https://doi.org/10.5194/egusphere-2026-2314
Preprint. Discussion started: 22 June 2026

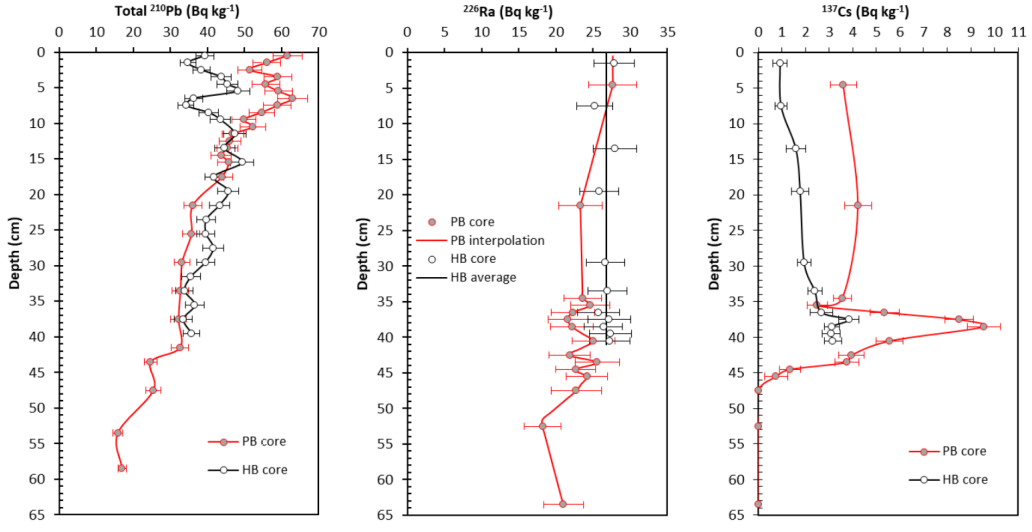

Fig. A4. Depth for total ^{210}Pb, ^{226}Ra and ^{137}Cs activities in marine short core HB (*Carnero-Bravo et al.*, 2021; *Falardeau et al., 2023b*) and a lagoon short core PB.

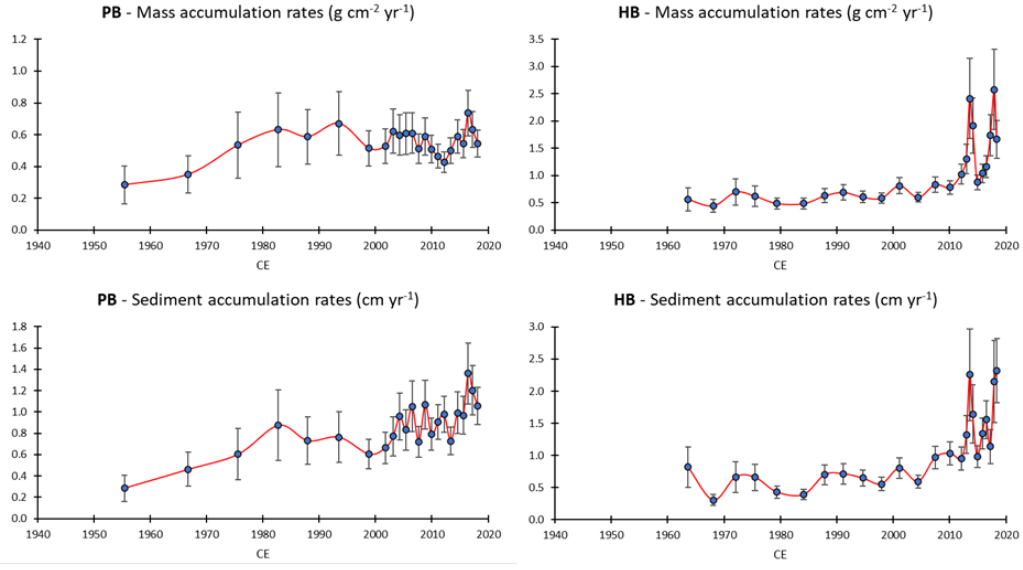

Fig. A5. Mean mass accumulation (MAR) and sediment accumulation rates (SAR) for the lagoon system Kanivaliuraq – Ptarmigan Bay lagoon (PB) and marine reference site Herschel Basin (HB). Error bars are standard deviations and come from Monte Carlo simulation.

https://doi.org/10.5194/egusphere-2026-2314
Preprint. Discussion started: 22 June 2026

Table A1. Location and information from short core collection.

Core	Short name	Location	Coordinates	Water depth (m)	Time of collection	Sampled with	Length (cm)
YC18-HB-GC01	HB	Herschel Basin	-138.97; 69.54435	18	August 2018	Gravity corer	38
YC18-PB-SC02	short core 1	Stream outlet, Ptarmigan Bay	-139.011; 69.56544	< 3	August 2018	Percussion corer	29
YC18-PB-SC01-A	short core 2	Central, Ptarmigan Bay	-139.085; 69.48251	3	August 2018	Percussion corer	23
YC18-PB-SC01	PB	Central, Ptarmigan Bay	-139.085; 69.48251	3	August 2018	Percussion corer	62

Table A2. Erosion and accretion rates for the Kanivaliuraq lagoon and Qikiqtaruk. Transects with significant erosion/accretion are the percentage of all transects that have a shoreline change rate larger than the uncertainty.

	1953-1972	1972-2011	2011-2018
Kanivaliuraq lagoon			
Mean shoreline change rate ± uncertainty (m yr^{-1})	-0.6 ± 0.8	-0.9 ± 0.8	-3.3 ± 0.7
Erosion			
Mean erosion rate (m yr^{-1})	-0.7	-0.9	-3.7
Maximum erosion rate (m yr^{-1})	-2.6	-3.4	-21.7
Transects with significant erosion (%)	29.8	64.5	70.6
Accretion			
Mean accretion rate (m yr^{-1})	0.3	0.2	0.7
Maximum accretion rate (m yr^{-1})	1.0	0.8	1.8
Transects with significant accretion (%)	0.4	3.3	3.4
Catton Point, Kanivaliuraq lagoon			
Mean shoreline change rate ± uncertainty (m yr^{-1})	-0.9 ± 0.8	-0.2 ± 0.3	-0.5 ± 0.7
Erosion			
Mean erosion rate (m yr^{-1})	-0.9	-0.2	-0.5
Maximum erosion rate (m yr^{-1})	-1.5	-0.4	-0.7
Transects with significant erosion (%)	50.0	25.0	0.0
Accretion			
Mean accretion rate (m yr^{-1})	-	-	-
Maximum accretion rate (m yr^{-1})	-	-	-
Transects with significant accretion (%)	0.0	0.0	0.0
Qikiqtaruk (south-east)			
Mean rate of shoreline change ± uncertainty (m yr^{-1})	NA	-0.6 ± 0.3	-0.7 ± 0.7
Erosion			
Mean erosion rate (m yr^{-1})	NA	-0.8	-0.7
Maximum erosion rate (m yr^{-1})	NA	-2.9	-5.8
Transects with significant erosion (%)	NA	67.7	47.4
Accretion			
Mean accretion rate (m yr^{-1})	NA	0.4	0.7
Maximum accretion rate (m yr^{-1})	NA	2.2	2.9
Transects with significant accretion (%)	NA	2.8	10.8

https://doi.org/10.5194/egusphere-2026-2314
Preprint. Discussion started: 22 June 2026

Data availability

Comment to the reviewers: all datasets were submitted to PANGAEA and are currently under review. By the time the manuscript will be published, all datasets will have an assigned DOI and be available online. In case you wish to take a look at the data beforehand, please contact the corresponding author, Anna Irrgang.

The following data sets were generated in this study and are available as a data collection on PANGAEA:

Dataset 1: Geochemical parameters of terrestrial sediment samples at the Yukon coast, Canada

Dataset 2: Geochemical parameters and sedimentological characteristics of lagoon sediments at the Yukon coast, Canada

Dataset 3: Geochemical parameters and sedimentological characteristics of marine sediments off the Yukon coast, Canada

Dataset 4: Radiometric (210Pb, 137 Cs) dating results and bulk mineralogy of lagoon sediment core off the Yukon coast, Canada

Dataset 5: Radiometric (210Pb, 137 Cs) dating results and bulk mineralogy of marine sediment core off the Yukon coast, Canada

The full citation will be: Tanski, George; Fritz, Michael; Vonk, Jorien E; Strauss, Jens; Chassiot, Léo; Carnero-Bravo, Vladislav; Falardeau, Jade; Hillaire-Marcel, Claude; Klein, Konstantin; Lantuit, Hugues; Speetjens, Niek J; de Vernal, Anne; Whalen, Dustin; Irrgang, Anna Maria (2026): Datasets on lateral and vertical organic matter fluxes in the Kanivaliuraq lagoon (Ptarmigan Bay) and Herschel Basin, western Canadian Arctic (dataset bundled publication). PANGAEA, https://doi.org/10.1594/PANGAEA.993352

Author contributions

Conceptualization: GT, MF, JEV, JS, AMI. Methodology: GT, JEV, VCB, KK, NJS, AMI. Funding and logistics: HL, JEV, MF. Writing – original draft preparation: GT, MF, JEV, JS, AMI. All authors contributed to the writing and reviewed the manuscript.

Competing interests

The contact author has declared that none of the authors has any competing interests.

Disclaimer

To be added by Copernicus

https://doi.org/10.5194/egusphere-2026-2314
Preprint. Discussion started: 22 June 2026

Acknowledgements

This project was conducted on indigenous lands in the Inuvialuit Settlement Region of northwestern Canada. We express our thanks and gratitude to the Yukon Territorial Government and particularly the park rangers of Qikiqtaruk – Herschel Island Territorial Parks for their enduring support. We further thank the Western Arctic Research Centre (WARC, Inuvik) for their logistical support and local guidance. We also thank Katharina Jaspers (AWI) for help with the technical aspects of the manuscript, Jan Kahl for supporting the logistics and Dyke Scheidemann for help with the lab work.

Financial support

This study received funding from the European Union's Horizon Program for the projects Nunataryuk (no. 773421) and ILLUQ (no. 101133587), the National Council of Science and Technology (CONACYT) postdoc grants from Mexico to Vladislav Carnero-Bravo (CVU no. 174856) and the Fonds de Recherche du Québec Nature et Technologies (FRQNT) doctoral scholarship to Jade Falardeau.

Review statement

To be added by Copernicus Publications

References

Abril-Hernández, J.M.: 210Pb-dating of sediments with models assuming a constant flux: CFCS, CRS, PLUM, and the novel χ-mapping. Review, performance tests, and guidelines, Journal of Environmental Radioactivity 268–269, 107248, https://doi.org/10.1016/j.jenvrad.2023.107248, 2023.

Airbus Defence and Space: Pléiades satellite imagery, acquired in 2018, Airbus Defence and Space, Toulouse, France, 2018.

Aller, R. C., and Blair, N. E.: Carbon remineralization in the Amazon–Guianas tropical mobile mudbelt: A sedimentary incinerator, Continental Shelf Research, 26, 2241–2259, https://doi.org/10.1016/j.csr.2006.07.016, 2006.

AMAP: AMAP Arctic Climate Change Update 2021: Key Trends and Impacts, Arctic Monitoring and Assessment Programme (AMAP), Tromsø, Norway, viii+148 pp, 2021.

Angelopoulos, M., Overduin, P. P., Westermann, S., Tronicke, J., Strauss, J., Schirrmeister, L., Biskaborn, B. K., Liebner, S., Maksimov, G., Grigoriev, M. N., and Grosse, G.: Thermokarst Lake to Lagoon Transitions in Eastern Siberia: Do Submerged Taliks Refreeze?, J. Geophys. Res.-Earth, 125, e2019JF005424, https://doi.org/10.1029/2019JF005424, 2020.

Angelopoulos, M., Overduin, P. P., Jenrich, M., Nitze, I., Günther, F., Strauss, J., Westermann, S., Schirrmeister, L., Kholodov, A., Krautblatter, M., Grigoriev, M. N., and Grosse, G.: Onshore Thermokarst Primes Subsea Permafrost Degradation, Geophys. Res. Lett., 48, e2021GL093881, https://doi.org/10.1029/2021GL093881, 2021.

Arndt, S., Jørgensen, B. B., LaRowe, D. E., Middelburg, J. J., Pancost, R. D., and Regnier, P.: Quantifying the degradation of organic matter in marine sediments: A review and synthesis, Earth-Sci. Rev., 123, 53–86, https://doi.org/10.1016/j.earscirev.2013.02.008, 2013.

Barnhart, K. R., Overeem, I., and Anderson, R. S.: The effect of changing sea ice on the physical vulnerability of Arctic coasts,

https://doi.org/10.5194/egusphere-2026-2314
Preprint. Discussion started: 22 June 2026

The Cryosphere, 8, 1777–1799, https://doi.org/10.5194/tc-8-1777-2014, 2014.

Bianchi, T. S.: The role of terrestrially derived organic carbon in the coastal ocean: a changing paradigm and the priming effect, P. Natl. Acad. Sci. USA, 108, 19473–19481, https://doi.org/10.1073/pnas.1017982108, 2011.

Bianchi, T. S., Arndt, S., Austin, W. E. N., Benn, D. I., Bertrand, S., Cui, X., Faust, J. C., Koziorowska-Makuch, K., Moy, C. M., Savage, C., Smeaton, C., Smith, R. W., and Syvitski, J.: Fjords as Aquatic Critical Zones (ACZs), Earth-Sci. Rev., 203, 103145, https://doi.org/10.1016/j.earscirev.2020.103145, 2020.

Biskaborn, B. K., Smith, S. L., Noetzli, J., Matthes, H., Vieira, G., Streletskiy, D. A., Schoeneich, P., Romanovsky, V. E., Lewkowicz, A. G., Abramov, A., Allard, M., Boike, J., Cable, W. L., Christiansen, H. H., Delaloye, R., Diekmann, B., Drozdov, D., Etzelmüller, B., Grosse, G., Guglielmin, M., Ingeman-Nielsen, T., Isaksen, K., Ishikawa, M., Johansson, M., Johannsson, H., Joo, A., Kaverin, D., Kholodov, A., Konstantinov, P., Kröger, T., Lambiel, C., Lanckman, J.-P., Luo, D., Malkova, G., Meiklejohn, I., Moskalenko, N., Oliva, M., Phillips, M., Ramos, M., Sannel, A. B. K., Sergeev, D., Seybold, C., Skryabin, P., Vasiliev, A., Wu, Q., Yoshikawa, K., Zheleznyak, M., and Lantuit, H.: Permafrost is warming at a global scale, Nat. Commun., 10, 264, https://doi.org/10.1038/s41467-018-08240-4, 2019.

Blott, S. J. and Pye, K.: GRADISTAT: a grain size distribution and statistics package for the analysis of unconsolidated sediments, Earth Surf. Proc. Land., 26, 1237–1248, https://doi.org/10.1002/esp.261, 2001.

Brunauer, S., Emmett, P. H., and Teller, E.: Adsorption of Gases in Multimolecular Layers, J. Am. Chem. Soc., 60, 309–319, https://doi.org/10.1021/ja01269a023, 1938.

Canadian Hydrographic Service: Canadian Tide and Current Tables, 4th edn., Fisheries and Oceans Canada, Ottawa, 96 pp, 2022.

Carmack, E. C. and Macdonald, R. W.: Oceanography of the Canadian Shelf of the Beaufort Sea: A Setting for Marine Life, Arctic, 55, 29–45, https://doi.org/10.14430/arctic733, 2002.

Carnero-Bravo, V., Falardeau, J., Chassiot, L., Tanski, G., Hillaire-Marcel, C., Ghaleb, B., Vernal, A. de, Vonk, J. E., Lantuit, H., Fritz, M., and Preda, M.: Sediment structure and deposition rates of sediment core YC18 HB GCO1, PANGAEA (data set), https://doi.org/10.1594/PANGAEA.937365, 2021.

Casas-Prat, M. and Wang, X. L.: Projections of Extreme Ocean Waves in the Arctic and Potential Implications for Coastal Inundation and Erosion, J. Geophys. Res.-Oceans, 125, e2019JC015745, https://doi.org/10.1029/2019JC015745, 2020.

Clark, J. B., Mannino, A., Tzortziou, M., Spencer, R. G. M., and Hernes, P. J.: The transformation and export of organic carbon across an Arctic river–delta–ocean continuum, Journal of Geophysical Research: Biogeosciences, 127, e2022JG007139, https://doi.org/10.1029/2022JG007139, 2022.

Coch, C., Lamoureux, S. F., Knoblauch, C., Eischeid, I., Fritz, M., Obu, J., and Lantuit, H.: Summer rainfall dissolved organic carbon, solute, and sediment fluxes in a small Arctic coastal catchment on Herschel Island (Yukon Territory, Canada), Arctic Science, 4, 750–780, https://doi.org/10.1139/as-2018-0010, 2018.

Coch, C., Juhls, B., Lamoureux, S. F., Lafrenière, M. J., Fritz, M., Heim, B., and Lantuit, H.: Comparisons of dissolved organic matter and its optical characteristics in small low and high Arctic catchments, Biogeosciences, 16, 4535–4553, https://doi.org/10.5194/bg-16-4535-2019, 2019.

Connolly, C. T., Cardenas, M. B., Burkart, G. A., Spencer, R. G. M., and McClelland, J. W.: Groundwater as a major source of dissolved organic matter to Arctic coastal waters, Nat. Commun., 11, 1479, https://doi.org/10.1038/s41467-020-15250-8, 2020.

https://doi.org/10.5194/egusphere-2026-2314
Preprint. Discussion started: 22 June 2026

Couture, N. J. and Pollard, W. H.: A Model for Quantifying Ground-Ice Volume, Yukon Coast, Western Arctic Canada, Permafrost Periglac., 28, 534–542, https://doi.org/10.1002/ppp.1952, 2017.

Couture, N. J., Irrgang, A., Pollard, W., Lantuit, H., and Fritz, M.: Coastal Erosion of Permafrost Soils Along the Yukon Coastal Plain and Fluxes of Organic Carbon to the Canadian Beaufort Sea, J. Geophys. Res.-Biogeo., 123, 406–422, https://doi.org/10.1002/2017JG004166, 2018.

Creel, R., Guimond, J., Jones, B. M., Nielsen, D. M., Bristol, E., Tweedie, C. E., and Overduin, P. P.: Permafrost thaw subsidence, sea-level rise, and erosion are transforming Alaska's Arctic coastal zone, P. Natl. Acad. Sci. USA, 121, e2409411121, https://doi.org/10.1073/pnas.2409411121, 2024.

Dunton, K. H., Weingartner, T., and Carmack, E. C.: The nearshore western Beaufort Sea ecosystem: Circulation and importance of terrestrial carbon in arctic coastal food webs, Prog. Oceanogr., 71, 362–378, https://doi.org/10.1016/j.pocean.2006.09.011, 2006.

Environment and Climate Change Canada: Historical Climate Data, Government of Canada (data set), 2022.

European Space Agency (ESA): Copernicus Sentinel-2 imagery, acquired in 2017, Copernicus Programme, European Space Agency, available at: https://dataspace.copernicus.eu/

Falardeau, J., Vernal, A. de, Fréchette, B., Hillaire-Marcel, C., Archambault, P., Fritz, M., Gallagher, C. P., and Tanski, G.: Impacts of stronger winds and less sea ice on Canadian Beaufort Sea shelf ecosystems since the late 1990s, Estuar. Coast. Shelf S., 294, 108520, https://doi.org/10.1016/j.ecss.2023.108520, 2023a.

Falardeau, J., de Vernal, A., Seidenkrantz, M.S., Cronin, T.-M., Gemery, L., Chassiot, L., Fritz, M., Carnero-Bravo, V., Hillaire-Marcel, C., and Archambault, P.: Microfaunal Recording of Recent Environmental Changes in the Herschel Basin, Western Arctic Ocean, Journal of Foraminiferal Research 53 (1): 20–48., https://doi.org/10.2113/gsjfr.53.1.20, 2023b.

Farquharson, L. M., Mann, D. H., Swanson, D. K., Jones, B. M., Buzard, R. M., and Jordan, J. W.: Temporal and spatial variability in coastline response to declining sea-ice in northwest Alaska, Mar. Geol., 404, 71–83, https://doi.org/10.1016/j.margeo.2018.07.007, 2018.

Forbes, D. L.: Coastal erosion and nearshore profile variability in the southern Beaufort Sea, Ivvavik National Park, Yukon Territory, Geological Survey of Canada, Dartmouth, Nova Scotia, Open File Rep. 3531, 102 pp, 1997.

Fritz, M., Wetterich, S., Schirrmeister, L., Meyer, H., Lantuit, H., Preusser, F., and Pollard, W. H.: Eastern Beringia and beyond: Late Wisconsinan and Holocene landscape dynamics along the Yukon Coastal Plain, Canada, Palaeogeogr. Palaeocl., 319–320, 28–45, https://doi.org/10.1016/j.palaeo.2011.12.015, 2012.

Fritz, M., Vonk, J. E., and Lantuit, H.: Collapsing Arctic coastlines, Nat. Clim. Change, 7, 6–7, https://doi.org/10.1038/nclimate3188, 2017.

GeoEye Inc.: GeoEye-1 satellite imagery, acquired in 2011, GeoEye Inc., Herndon, Virginia, USA, 2011.

Gonçalves-Araujo, R., Stedmon, C. A., Heim, B., Dubinenkov, I., Kraberg, A., Moiseev, D., and Bracher, A.: From Fresh to Marine Waters: Characterization and Fate of Dissolved Organic Matter in the Lena River Delta Region, Siberia, Front. Mar. Sci., 2, 170808, https://doi.org/10.3389/fmars.2015.00108, 2015.

Goñi, M. A., Yunker, M. B., Macdonald, R. W., and Eglinton, T. I.: Distribution and sources of organic biomarkers in arctic sediments from the Mackenzie River and Beaufort Shelf, Mar. Chem., 71, 23–51, https://doi.org/10.1016/S0304-4203(00)00037-2, 2000.

https://doi.org/10.5194/egusphere-2026-2314
Preprint. Discussion started: 22 June 2026

Grotheer, H., Meyer, V. D., Riedel, T., Pfalz, G., Mathieu, L., Hefter, J., Gentz, T., Lantuit, H., Mollenhauer, G., and Fritz, M.: Burial and origin of permafrost derived carbon in the nearshore zone of the southern Canadian Beaufort Sea, PANGAEA (data set), https://doi.org/10.1594/PANGAEA.910013, 2019.

Grotheer, H., Meyer, V., Riedel, T., Pfalz, G., Mathieu, L., Hefter, J., Gentz, T., Lantuit, H., Mollenhauer, G., and Fritz, M.: Burial and Origin of Permafrost-Derived Carbon in the Nearshore Zone of the Southern Canadian Beaufort Sea, Geophys. Res. Lett., 47, e2019GL085897, https://doi.org/10.1029/2019GL085897, 2020.

Hanna, A. J., Allison, M. A., Bianchi, T. S., Marcantonio, F., and Goff, J. A.: Late Holocene sedimentation in a high Arctic coastal setting: Simpson Lagoon and Colville Delta, Alaska, Cont. Shelf Res., 74, 11–24, https://doi.org/10.1016/j.csr.2013.11.026, 2014.

Harris, C. M., McClelland, J. W., Connelly, T. L., Crump, B. C., and Dunton, K. H.: Salinity and Temperature Regimes in Eastern Alaskan Beaufort Sea Lagoons in Relation to Source Water Contributions, Estuar. Coast, 40, 50–62, https://doi.org/10.1007/s12237-016-0123-z, 2017.

Harris, C. M., McTigue, N. D., McClelland, J. W., and Dunton, K. H.: Do high Arctic coastal food webs rely on a terrestrial carbon subsidy?, Food Webs, 15, e00081, https://doi.org/10.1016/j.fooweb.2018.e00081, 2018.

Héquette, A. and Barnes, P. W.: Coastal retreat and shoreface profile variations in the Canadian Beaufort Sea, Mar. Geol., 91, 113–132, https://doi.org/10.1016/0025-3227(90)90136-8, 1990.

Héquette, A., Ruz, M.-H., and Hill, P. R.: The Effects of the Holocene Sea Level Rise on the Evolution of the Southeastern Coast of the Canadian Beaufort Sea, J. Coastal Res., 11, 494–507, 1995.

Hill, P. R., Blasco, S. M., Harper, J. R., and Fissel, D. B.: Sedimentation on the Canadian Beaufort Shelf, Cont. Shelf Res., 11, 821–842, https://doi.org/10.1016/0278-4343(91)90081-G, 1991.

Himmelstoss, E. A., Henderson, R. E., Kratzmann, M. G., and Farris, A. S.: Digital Shoreline Analysis System (DSAS) Version 5.0 User Guide, U.S. Geological Survey, Reston, USA, Open File Rep. 2018-1179, 110 pp, 2018.

Irrgang, A. M., Lantuit, H., Manson, G. K., Günther, F., Grosse, G., and Overduin, P. P.: Variability in Rates of Coastal Change Along the Yukon Coast, 1951 to 2015, J. Geophys. Res.-Earth, 123, 779–800, https://doi.org/10.1002/2017JF004326, 2018.

Irrgang, A. M., Bendixen, M., Farquharson, L. M., Baranskaya, A. V., Erikson, L. H., Gibbs, A. E., Ogorodov, S. A., Overduin, P. P., Lantuit, H., Grigoriev, M. N., and Jones, B. M.: Drivers, dynamics and impacts of changing Arctic coasts, Nat. Rev. Earth Environ., 3, 39–54, https://doi.org/10.1038/s43017-021-00232-1, 2022.

Jenrich, M., Angelopoulos, M., Grosse, G., Overduin, P. P., Schirrmeister, L., Nitze, I., Biskaborn, B. K., Liebner, S., Grigoriev, M., Murray, A., Jongejans, L. L., and Strauss, J.: Thermokarst Lagoons: A Core-Based Assessment of Depositional Characteristics and an Estimate of Carbon Pools on the Bykovsky Peninsula, Front. Earth Sci., 9, 637899, https://doi.org/10.3389/feart.2021.637899, 2021.

Jenrich, M., Angelopoulos, M., Liebner, S., Treat, C., Knoblauch, C., Yang, S., Grosse, G., Giebeler, F., Jongejans, L. L., Grigoriev, M., and Strauss, J.: Greenhouse Gas Production and Microbial Response During the Transition From Terrestrial Permafrost to a Marine Environment, Permafrost Periglac., 36, 63–82, https://doi.org/10.1002/ppp.2251, 2025a.

Jenrich, M., Wolter, J., Liebner, S., Knoblauch, C., Grosse, G., Giebeler, F., Whalen, D., and Strauss, J.: Rising Arctic seas and thawing permafrost: uncovering the carbon cycle impact in a thermokarst lagoon system in the outer Mackenzie Delta, Canada, Biogeosciences, 22, 2069–2086, https://doi.org/10.5194/bg-22-2069-2025, 2025b.

https://doi.org/10.5194/egusphere-2026-2314
Preprint. Discussion started: 22 June 2026

Jenrich, M., Prodinger, M., Nitze, I., Grosse, G., and Strauss, J.: Thermokarst Lagoons: Distribution, Classification and Dynamics in Permafrost-to-Marine Transitions, Permafrost Periglac., 1–16, https://doi.org/10.1002/ppp.70001, 2025c.

Jones, B. M., Arp, C. D., Beck, R. A., Grosse, G., Webster, J. M., and Urban, F. E.: Erosional history of Cape Halkett and contemporary monitoring of bluff retreat, Beaufort Sea coast, Alaska, Polar Geogr., 32, 129–142, https://doi.org/10.1080/10889370903486449, 2009.

Jones, B. M., Farquharson, L. M., Baughman, C. A., Buzard, R. M., Arp, C. D., Grosse, G., Bull, D. L., Günther, F., Nitze, I., Urban, F., Kasper, J. L., Frederick, J. M., Thomas, M., Jones, C., Mota, A., Dallimore, S., Tweedie, C., Maio, C., Mann, D. H., Richmond, B., Gibbs, A., Xiao, M., Sachs, T., Iwahana, G., Kanevskiy, M., and Romanovsky, V. E.: A decade of remotely sensed observations highlight complex processes linked to coastal permafrost bluff erosion in the Arctic, Environ. Res. Lett., 13, 115001, https://doi.org/10.1088/1748-9326/aae471, 2018.

Jong, D., Bröder, L., Tanski, G., Fritz, M., Lantuit, H., Tesi, T., Haghipour, N., Eglinton, T. I., and Vonk, J. E.: Nearshore Zone Dynamics Determine Pathway of Organic Carbon From Eroding Permafrost Coasts, Geophys. Res. Lett., 47, e2020GL088561, https://doi.org/10.1029/2020GL088561, 2020.

Jong, D., Bröder, L., Tesi, T., Tanski, G., Oudenhuijsen, M., Fritz, M., and Vonk, J. E.: Selective sorting and degradation of permafrost organic matter in the nearshore zone of Herschel Island (Yukon, Canada), Journal of Geophysical Research: Biogeosciences, 129, e2023JG007479, https://doi.org/10.1029/2023JG007479, 2024.

Jorgenson, M. T. and Brown, J.: Classification of the Alaskan Beaufort Sea Coast and estimation of carbon and sediment inputs from coastal erosion, Geo-Mar. Lett., 25, 69–80, https://doi.org/10.1007/s00367-004-0188-8, 2005.

Juhls, B., Matsuoka, A., Lizotte, M., Bécu, G., Overduin, P. P., El Kassar, J., Devred, E., Doxaran, D., Ferland, J., Forget, M. H., Hilborn, A., Hieronymi, M., Leymarie, E., Maury, J., Oziel, L., Tisserand, L., Anikina, D., Dillon, M., and Babin, M.: Seasonal dynamics of dissolved organic matter in the Mackenzie Delta, Canadian Arctic waters: Implications for ocean colour remote sensing, Remote Sens. Environ., 283, 113327, https://doi.org/10.1016/j.rse.2022.113327, 2022.

Keil, R. G., Mayer, L. M., Quay, P. D., Richey, J. E., and Hedges, J. I.: Loss of organic matter from riverine particles in deltas, Geochim. Cosmochim. Acta, 61, 1507–1511, https://www.sciencedirect.com/science/article/abs/pii/S0016703797000446, 1997.

Klein, K. P., Lantuit, H., Heim, B., Fell, F., Doxaran, D., and Irrgang, A. M.: Long-Term High-Resolution Sediment and Sea Surface Temperature Spatial Patterns in Arctic Nearshore Waters Retrieved Using 30-Year Landsat Archive Imagery, Remote Sens.-Basel, 11, 2791, https://doi.org/10.3390/rs11232791, 2019.

Klein, K. P., Lantuit, H., Heim, B., Doxaran, D., Juhls, B., Nitze, I., Walch, D., Poste, A., and Søreide, J. E.: The Arctic Nearshore Turbidity Algorithm (ANTA) - A multi sensor turbidity algorithm for Arctic nearshore environments, Science of Remote Sensing, 4, 100036, https://doi.org/10.1016/j.srs.2021.100036, 2021.

Knoblauch, C., Beer, C., Sosnin, A., Wagner, D., and Pfeiffer, E.-M.: Predicting long-term carbon mineralization and trace gas production from thawing permafrost of Northeast Siberia, Global Change Biol., 19, 1160–1172, https://doi.org/10.1111/gcb.12116, 2013.

Kuzyk, Z. Z. A., Gobeil, C., and Macdonald, R. W.: 210 Pb and 137 Cs in margin sediments of the Arctic Ocean: Controls on boundary scavenging, Global Biogeochem. Cy., 27, 422–439, https://doi.org/10.1002/gbc.20041, 2013.

Krylenko, V.: Estuaries and Lagoons of the Russian Arctic Seas. In: Kosyan, R. (eds) The Diversity of Russian Estuaries and

https://doi.org/10.5194/egusphere-2026-2314
Preprint. Discussion started: 22 June 2026

Lagoons Exposed to Human Influence. Estuaries of the World. Springer, Cham. https://doi.org/10.1007/978-3-319-43392-9_2, 2017

Lavoie, D., Macdonald, R. W., and Denman, K. L.: Primary productivity and export fluxes on the Canadian shelf of the Beaufort Sea: A modelling study, in: J. Marine Syst., 75 (1-2), 17-32, https://doi.org/10.1016/j.jmarsys.2008.07.007, 2009.

Lee, H., Schuur, E. A. G., Inglett, K. S., Lavoie, M., and Chanton, J. P.: The rate of permafrost carbon release under aerobic and anaerobic conditions and its potential effects on climate, Global Change Biol., 18, 515–527, https://doi.org/10.1111/j.1365-2486.2011.02519.x, 2012.

Macdonald, R. W., Solomon, S. M., Cranston, R. E., Welch, H. E., Yunker, M. B., and Gobeil, C.: A sediment and organic carbon budget for the Canadian Beaufort Shelf, Mar. Geol., 144, 255–273, https://doi.org/10.1016/S0025-3227(97)00106-0, 1998.

Macdonald, R. W., Kuzyk, Z. Z. A., and Johannessen, S. C.: The vulnerability of Arctic shelf sediments to climate change, Environ. Rev., 23, 461–479, https://doi.org/10.1139/er-2015-0040, 2015.

Mackay, J. R.: Glacier ice-thrust features of the Yukon coast, Geographical Bulletin, 13, 5–21, https://doi.org/10.4095/331056, 1959.

Mackelprang, R., Waldrop, M. P., DeAngelis, K. M., David, M. M., Chavarria, K. L., Blazewicz, S. J., Rubin, E. M., and Jansson, J. K.: Metagenomic analysis of a permafrost microbial community reveals a rapid response to thaw, Nature, 480, 368–371, https://doi.org/10.1038/nature10576, 2011.

Magen, C., Chaillou, G., Crowe, S. A., Mucci, A., Sundby, B., Gao, A., Makabe, R., and Sasaki, H.: Origin and fate of particulate organic matter in the southern Beaufort Sea – Amundsen Gulf region, Canadian Arctic, Estuar. Coast. Shelf S., 86, 31–41, https://doi.org/10.1016/j.ecss.2009.09.009, 2010.

Manson, G. K. and Solomon, S. M.: Past and future forcing of Beaufort Sea coastal change, Atmos. Ocean, 45, 107–122, https://doi.org/10.3137/ao.450204, 2007.

Matsuoka, A., Bricaud, A., Benner, R., Para, J., Sempéré, R., Prieur, L., Bélanger, S., and Babin, M.: Tracing the transport of colored dissolved organic matter in water masses of the Southern Beaufort Sea: relationship with hydrographic characteristics, Biogeosciences, 9, 925–940, https://doi.org/10.5194/bg-9-925-2012, 2012.

Miesner, F., Overduin, P. P., Grosse, G., Strauss, J., Langer, M., Westermann, S., Schneider von Deimling, T., Brovkin, V., and Arndt, S.: Subsea permafrost organic carbon stocks are large and of dominantly low reactivity, Sci. Rep.-UK, 13, 9425, https://doi.org/10.1038/s41598-023-36471-z, 2023.

Miller, C. A., Bonsell, C., McTigue, N. D., and Kelley, A. L.: The seasonal phases of an Arctic lagoon reveal the discontinuities of pH variability and CO2 flux at the air–sea interface, Biogeosciences, 18, 1203–1221, https://doi.org/10.5194/bg-18-1203-2021, 2021.

Mitzscherling, J., Winkel, M., Winterfeld, M., Horn, F., Yang, S., Grigoriev, M. N., Wagner, D., Overduin, P. P., and Liebner, S.: The development of permafrost bacterial communities under submarine conditions, J. Geophys. Res.-Biogeo., 122, 1689–1704, https://doi.org/10.1002/2017JG003859, 2017.

Morrissey, E. M., Gillespie, J. L., Morina, J. C., and Franklin, R. B.: Salinity affects microbial activity and soil organic matter content in tidal wetlands, Global Change Biol., 20, 1351–1362, https://doi.org/10.1111/gcb.12431, 2014.

Naidu, A. S., Cooper, L. W., Finney, B. P., Macdonald, R. W., Alexander, C., and Semiletov, I. P.: Organic carbon isotope ratios (δ 13 C) of Arctic Amerasian Continental shelf sediments, Int. J. Earth Sci., 89, 522–532,

https://doi.org/10.5194/egusphere-2026-2314
Preprint. Discussion started: 22 June 2026

https://doi.org/10.1007/s005310000121, 2000.

Natali, S. M., Watts, J. D., Rogers, B. M., Potter, S., Ludwig, S. M., Selbmann, A.-K., Sullivan, P. F., Abbott, B. W., Arndt, K. A., Birch, L., Björkman, M. P., Bloom, A. A., Celis, G., Christensen, T. R., Christiansen, C. T., Commane, R., Cooper, E. J., Crill, P., Czimczik, C., Davydov, S., Du, J., Egan, J. E., Elberling, B., Euskirchen, E. S., Friborg, T., Genet, H., Göckede, M., Goodrich, J. P., Grogan, P., Helbig, M., Jafarov, E. E., Jastrow, J. D., Kalhori, A. A. M., Kim, Y., Kimball, J., Kutzbach, L., Lara, M. J., Larsen, K. S., Lee, B.-Y., Liu, Z., Loranty, M. M., Lund, M., Lupascu, M., Madani, N., Malhotra, A., Matamala, R., McFarland, J., McGuire, A. D., Michelsen, A., Minions, C., Oechel, W. C., Olefeldt, D., Parmentier, F.-J. W., Pirk, N., Poulter, B., Quinton, W., Rezanezhad, F., Risk, D., Sachs, T., Schaefer, K., Schmidt, N. M., Schuur, E. A. G., Semenchuk, P. R., Shaver, G., Sonnentag, O., Starr, G., Treat, C. C., Waldrop, M. P., Wang, Y., Welker, J., Wille, C., Xu, X., Zhang, Z., Zhuang, Q., and Zona, D.: Large loss of CO2 in winter observed across the northern permafrost region, Nat. Clim. Change, 9, 852–857, https://doi.org/10.1038/s41558-019-0592-8, 2019.

Nielsen, D. M., Pieper, P., Barkhordarian, A., Overduin, P., Ilyina, T., Brovkin, V., Baehr, J., and Dobrynin, M.: Increase in Arctic coastal erosion and its sensitivity to warming in the twenty-first century, Nat. Clim. Change, 12, 263–270, https://doi.org/10.1038/s41558-022-01281-0, 2022.

Obu, J., Lantuit, H., Fritz, M., Pollard, W. H., Sachs, T., and Günther, F.: Relation between planimetric and volumetric measurements of permafrost coast erosion: a case study from Herschel Island, western Canadian Arctic, Polar Res., 35, 30313, https://doi.org/10.3402/polar.v35.30313, 2016.

Obu, J., Lantuit, H., Grosse, G., Günther, F., Sachs, T., Helm, V., and Fritz, M.: Coastal erosion and mass wasting along the Canadian Beaufort Sea based on annual airborne LiDAR elevation data, Geomorphology, 293, 331–346, https://doi.org/10.1016/j.geomorph.2016.02.014, 2017.

Osterkamp, T. E., Baker, G. C., Harrison, W. D., and Matava, T.: Characteristics of the active layer and shallow subsea permafrost, J. Geophys. Res.-Oceans, 94, 16227–16236, https://doi.org/10.1029/JC094iC11p16227, 1989.

Overeem, I., Anderson, R. S., Wobus, C. W., Clow, G. D., Urban, F. E., and Matell, N.: Sea ice loss enhances wave action at the Arctic coast, Geophys. Res. Lett., 38, L17503, https://doi.org/10.1029/2011GL048681, 2011.

Pelletier, B. R.: Marine science atlas of the Beaufort Sea : geology and geophysics (Map). Minister of Supply and Services Canada, 1987.

Pelletier, B. R. and Medioli, B. E. (Eds.): Environmental atlas of the Beaufort coastlands, Geological Survey of Canada, Open File Rep. 7619, 271 pp, https://doi.org/10.4095/294601, 2014.

Radosavljevic, B., Lantuit, H., Knoblauch, C., Couture, N., Herzschuh, U., and Fritz, M.: Arctic Nearshore Sediment Dynamics—An Example from Herschel Island—Qikiqtaruk, Canada, J. Mar. Sci. Eng., 10, 1589, https://doi.org/10.3390/jmse10111589, 2022.

Ramage, J. L., Irrgang, A. M., Morgenstern, A., and Lantuit, H.: Increasing coastal slump activity impacts the release of sediment and organic carbon into the Arctic Ocean, Biogeosciences, 15, 1483–1495, https://doi.org/10.5194/bg-15-1483-2018, 2018.

Rampton, V. N.: Quaternary geology of the Yukon Coastal Plain, Geological Survey of Canada, Bulletin, Ottawa, Canada, 61 pp, 1982.

Rantanen, M., Karpechko, A. Y., Lipponen, A., Nordling, K., Hyvärinen, O., Ruosteenoja, K., Vihma, T., and Laaksonen, A.: The Arctic has warmed nearly four times faster than the globe since 1979, Commun. Earth Environ., 3, 1–10,

https://doi.org/10.5194/egusphere-2026-2314
Preprint. Discussion started: 22 June 2026

https://doi.org/10.1038/s43247-022-00498-3, 2022.

Rößger, N., Sachs, T., Wille, C., Boike, J., and Kutzbach, L.: Seasonal increase of methane emissions linked to warming in Siberian tundra, Nat. Clim. Change, 12, 1031–1036, https://doi.org/10.1038/s41558-022-01512-4, 2022.

Sanchez-Cabeza, J. A. and Ruiz-Fernández, A. C.: 210Pb sediment radiochronology: An integrated formulation and classification of dating models, Geochim. Cosmochim. Ac., 82, 183–200, https://doi.org/10.1016/j.gca.2010.12.024, 2012.

Sanchez-Cabeza, J.-A., Ruiz-Fernández, A. C., Ontiveros-Cuadras, J. F., Pérez Bernal, L. H., and Olid, C.: Monte Carlo uncertainty calculation of 210Pb chronologies and accumulation rates of sediments and peat bogs, Quaternary Geochronology, 23, 80–93, https://doi.org/10.1016/j.quageo.2014.06.002, 2014.

Schirrmeister, L., Grigoriev, M. N., Strauss, J., Grosse, G., Overduin, P. P., Kholodov, A., Guenther, F., and Hubberten, H.-W.: Sediment characteristics of a thermokarst lagoon in the northeastern Siberian Arctic (Ivashkina Lagoon, Bykovsky Peninsula), Arktos, 4, 1–16, https://doi.org/10.1007/s41063-018-0049-8, 2018.

Schreiner, K. M., Bianchi, T. S., Eglinton, T. I., Allison, M. A., and Hanna, A. J. M.: Sources of terrigenous inputs to surface sediments of the Colville River Delta and Simpson's Lagoon, Beaufort Sea, Alaska, J. Geophys. Res., 118, 808–824, https://doi.org/10.1002/jgrg.20065, 2013.

Schuur, E. A., Abbott, B. W., Commane, R., Ernakovich, J., Euskirchen, E., Hugelius, G., Grosse, G., Jones, M., Koven, C., Leshyk, V., Lawrence, D., Loranty, M. M., Mauritz, M., Olefeldt, D., Natali, S., Rodenhizer, H., Salmon, V., Schädel, C., Strauss, J., Treat, C., and Turetsky, M.: Permafrost and Climate Change: Carbon Cycle Feedbacks From the Warming Arctic, Annu. Rev. Env. Resour., 47, 343–371, https://doi.org/10.1146/annurev-environ-012220-011847, 2022.

Solomon, S., Mudie, P. J., Cranston, R., Hamilton, T., Thibaudeau, S. A., and Collins, E. S.: Characterisation of marine and lacustrine sediments in a drowned thermokarst embayment, Richards Island, Beaufort Sea, Canada, Int. J. Earth Sci., 89, 503–521, https://doi.org/10.1007/s005310000126, 2000.

Speetjens, N. J., Tanski, G., Martin, V., Wagner, J., Richter, A., Hugelius, G., Boucher, C., Lodi, R., Knoblauch, C., Koch, B. P., Wünsch, U., Lantuit, H., and Vonk, J. E.: Dissolved organic matter characterization in soils and streams in a small coastal low-Arctic catchment, Biogeosciences, 19, 3073–3097, https://doi.org/10.5194/bg-19-3073-2022, 2022.

Strauss, J., Schirrmeister, L., Grosse, G., Wetterich, S., Ulrich, M., Herzschuh, U., and Hubberten, H.-W.: The deep permafrost carbon pool of the Yedoma region in Siberia and Alaska, Geophys. Res. Lett., 40, 6165–6170, https://doi.org/10.1002/2013GL058088, 2013.

Strauss, J., Fuchs, M., Hugelius, G., Miesner, F., Nitze, I., Opfergelt, S., Schuur, E., Treat, C., Turetsky, M., Yang, Y., and Grosse, G.: Organic matter storage and vulnerability in the permafrost domain, in: Encyclopedia of Quaternary Science, 3rd edn., edited by: Elias, S. A., Elsevier, San Diego, USA, 399–410, 2025.

Tank, S. E., Striegl, R. G., McClelland, J. W., and Kokelj, S. V.: Multi-decadal increases in dissolved organic carbon and alkalinity flux from the Mackenzie drainage basin to the Arctic Ocean, Environ. Res. Lett., 11, 54015, https://doi.org/10.1088/1748-9326/11/5/054015, 2016.

Tanski, G., Lantuit, H., Ruttor, S., Knoblauch, C., Radosavljevic, B., Strauss, J., Wolter, J., Irrgang, A. M., Ramage, J., and Fritz, M.: Transformation of terrestrial organic matter along thermokarst-affected permafrost coasts in the Arctic, Sci. Total Environ., 581–582, 434–447, https://doi.org/10.1016/j.scitotenv.2016.12.152, 2017.

Tanski, G., Wagner, D., Knoblauch, C., Fritz, M., Sachs, T., and Lantuit, H.: Rapid CO2 Release From Eroding Permafrost in

https://doi.org/10.5194/egusphere-2026-2314
Preprint. Discussion started: 22 June 2026

Seawater, Geophys. Res. Lett., 46, 11244–11252, https://doi.org/10.1029/2019GL084303, 2019.

Turetsky, M. R., Abbott, B. W., Jones, M. C., Anthony, K. W., Olefeldt, D., Schuur, E. A. G., Grosse, G., Kuhry, P., Hugelius, G., Koven, C., Lawrence, D. M., Gibson, C., Sannel, A. B. K., and McGuire, A. D.: Carbon release through abrupt permafrost thaw, Nat. Geosci., 13, 138–143, https://doi.org/10.1038/s41561-019-0526-0, 2020.

USGS Earth Explorer: https://earthexplorer.usgs.gov, last access: 26 August 2025.

van Crimpen, F. C. J., Madaj, L., Whalen, D., Tesi, T., van Genuchten, J. M., Bröder, L., Eglinton, T. I., Haghipour, N., and Vonk, J. E.: Traveling Light: Arctic Coastal Erosion Releases Mostly Matrix Free, Unprotected Organic Carbon, Geophys. Res. Lett., 51, e2024GL108622, https://doi.org/10.1029/2024GL108622, 2024.

Vanhellemont, Q.: Adaptation of the dark spectrum fitting atmospheric correction for aquatic applications of the Landsat and Sentinel-2 archives, Remote Sens. Environ., 225, 175–192, https://doi.org/10.1016/j.rse.2019.03.010, 2019.

Vonk, J. E., Sánchez-García, L., van Dongen, B. E., Alling, V., Kosmach, D., Charkin, A., Semiletov, I. P., Dudarev, O. V., Shakhova, N., Roos, P., Eglinton, T. I., Andersson, A., and Gustafsson, O.: Activation of old carbon by erosion of coastal and subsea permafrost in Arctic Siberia, Nature, 489, 137–140, https://doi.org/10.1038/nature11392, 2012.

Vonk, J. E., Fritz, M., Speetjens, N. J., Babin, M., Bartsch, A., Basso, L. S., Bröder, L., Göckede, M., Gustafsson, Ö., Hugelius, G., Irrgang, A. M., Juhls, B., Kuhn, M. A., Lantuit, H., Manizza, M., Martens, J., O'Regan, M., Suslova, A., Tank, S. E., Terhaar, J., and Zolkos, S.: The land–ocean Arctic carbon cycle, Nat. Rev. Earth Environ., 6, 86–105, https://doi.org/10.1038/s43017-024-00627-w, 2025.

Wegner, C., Bennett, K. E., Vernal, A. de, Forwick, M., Fritz, M., Heikkilä, M., Łącka, M., Lantuit, H., Laska, M., Moskalik, M., O'Regan, M., Pawłowska, J., Promińska, A., Rachold, V., Vonk, J. E., and Werner, K.: Variability in transport of terrigenous material on the shelves and the deep Arctic Ocean during the Holocene, Polar Res., 34, 24964, https://doi.org/10.3402/polar.v34.24964, 2015.

Weiss, N. and Kaal, J.: Characterization of labile organic matter in Pleistocene permafrost (NE Siberia), using Thermally assisted Hydrolysis and Methylation (THM-GC-MS), Soil Bio. Biochem., 117, 203–213, https://doi.org/10.1016/j.soilbio.2017.10.001, 2018.

Winkel, M., Sepulveda-Jauregui, A., Martinez-Cruz, K., Heslop, J. K., Rijkers, R., Horn, F., Liebner, S., and Walter Anthony, K. M.: First evidence for cold-adapted anaerobic oxidation of methane in deep sediments of thermokarst lakes, Environ. Res. Commun., 1, 21002, https://doi.org/10.1088/2515-7620/ab1042, 2019.

Wukelic, G. E., Gibbons, D. E., Martucci, L. M., and Foote, H. P.: Radiometric calibration of Landsat Thematic Mapper thermal band, Remote Sens. Environ., 28, 339–347, https://doi.org/10.1016/0034-4257(89)90125-9, 1989.

Zhang, Y., Li, Y., Wang, L., Tang, Y., Chen, J., Hu, Y., Fu, X., and Le, Y.: Soil microbiological variability under different successional stages of the Chongming Dongtan wetland and its effect on soil organic carbon storage, Ecol. Eng., 52, 308–315, https://doi.org/10.1016/j.ecoleng.2012.10.002, 2013.